MIXED METHODS FOR THE VELOCITY-PRESSURE-PSEUDOSTRESS FORMULATION OF THE STOKES EIGENVALUE PROBLEM*

FELIPE LEPE†, GONZALO RIVERA‡, AND JESUS VELLOJIN§

Abstract. In two and three dimensions, we analyze mixed finite element methods for a velocity-pressure-pseudostress formulation of the Stokes eigenvalue problem. The methods consist in two schemes: the velocity and pressure are approximated with piecewise polynomial, whereas for the pseudostress we consider two classic families of finite elements for H(div) spaces: the Raviart-Thomas and the Brezzi-Douglas-Marini elements. With the aid of the classic spectral theory for compact operators, we prove that our method does not introduce spurious modes. Also, we obtain convergence and error estimates for the proposed methods. We report numerical results to compare the accuracy and robustness between both numerical schemes.

Key words. Stokes equations, eigenvalue problems, error estimates

AMS subject classifications. 35Q35, 65N15, 65N25, 65N30, 65N50, 76D07

1. Introduction.

The Stokes problem is a system of equations that describes the motion of a certain fluid. For a given domain $\Omega \subset \mathbb{R}^n$, where $n \in \{2, 3\}$ with Lipschitz boundary, we are interested in the Stokes eigenvalue problem

$$\left\{ \begin{array}{rcll} -2\mu\Delta \boldsymbol{u} + \nabla p &=& \lambda \boldsymbol{u} & \text{in} \quad \Omega, \\ \operatorname{div} \boldsymbol{u} &=& 0 & \text{in} \quad \Omega, \\ \boldsymbol{u} &=& \boldsymbol{0} & \text{on} \quad \partial\Omega, \end{array} \right. \tag{1.1}$$

where μ is the kinematic viscosity, $\boldsymbol{u}$ is the velocity and p is the pressure.

It is well known that mixed formulations are a suitable alternative to analyze different problems, since the introduction of additional unknowns with physical meaning allows to obtain more information on certain phenomena. Hence, the design of finite element approximations has been an important subject of study for mathematicians and engineers, where several families of mixed elements have been developed. For a complete state of art about mixed methods we resort to [5].

In particular, mixed formulations for eigenvalue problems has been well developed in the past years and the theory to study these problems can be found in [4, 28], just to mention the most classic references. On the other hand, concrete applications for mixed formulations in spectral problems can be found in different contexts as, for instance, [2, 14, 17, 16, 20, 22, 23], where an amount of numerical approaches such as DG methods, VEM methods, FEM, or a posteriori analysis, have been implemented.

We mention that the Stokes eigenvalue problem has attracted much interest since it is frequently encountered in important applications, for instance, to study the

*Submitted to the editors DATE.

Funding: The first author was partially supported by DIUBB through project 2120173 GI/C Universidad del Bío-Bío and ANID-Chile through FONDECYT project 11200529 (Chile). The second author was supported by ANID-Chile through FONDECYT project 11170534 (Chile). The third author was partially supported by ANID-Chile through FONDECYT project 1181098 (Chile).

†GIMNAP-Departamento de Matemática, Universidad del Bío - Bío, Casilla 5-C, Concepción, Chile. flepe@ubiobio.cl.

‡Departamento de Ciencias Exactas, Universidad de Los Lagos, Casilla 933, Osorno, Chile. gonzalo.rivera@ulagos.cl.

§Departamento de Matemática, Universidad Técnica Federico Santa María, Valparaíso, Chile. jesus.vellojinm@usm.cl.

stability of fluid flow problems, and it also appears in the analysis of the elastic stability of thin plates [29, 28], reinforcing the importance of the accuracy when the eigenmodes of the Stokes spectral system are computed.

In the present work, we consider a mixed formulation for the Stokes spectral problem that incorporates the so-called nonsymmetric pseudotress tensor (see [11] for further details related to this tensor) which is a suitable unknown in order to eliminate the pressure and velocity from the PDE system, leading to an elliptic problem as is analyzed in [26, 21].

Now, in our work, we do not eliminate these variables and consider a more complete system where the pseudotress, the pressure and velocity are part of the system, leading to a mixed formulation that is numerically analyzed with inf-sup stable families of finite elements. With this new approach for the Stokes eigensystem, instead of recovering the velocity and pressure with a postprocess as in [26], we are able to obtain these unknowns directly by using standard eigensolvers.

More precisely, we will study the Stokes eigenvalue problem with the mixed formulation proposed in [15], already analyzed for the source problem, where not only the velocity and the pressure are the unknowns as in (1.1), but also the pseudostress tensor. With this formulation, it is expected that the computational costs for the numerical methods increase, when compared to the classic velocity-pressure formulation, since we need to approximate each component of the pseudostress, each component of the velocity, and the scalar associated to the pressure. However, the choice of appropriate discrete spaces might compensate for the increase in degrees of freedom. In addition, the pseudostress tensor is an interesting unknown, because it allows to compute other quantities of interest. For example, in the Stokes flow problems, the pseudostress relates the classic stress and the gradient of the velocity. Hence, with an accurate approximation of the pseudostress we are able to obtain accurate values for these other important unknowns that might be desired in certain applications.

Whereas the computational costs are an important subject, the regularity for the eigenfunctions with the formulation presented in this work is less restrictive when compared, for instance, to [26], since the H(div) space does not need to be split in a direct sum. In fact, the classic regularity results for the velocity-pressure formulation can be used straightforwardly in order to obtain additional regularity for the pseudotress tensor. Besides, mixed formulations are flexible in the choice of finite element families to approximate the space H(div). In our case, we consider two families: the Raviart-Thomas elements and the Brezzi-Douglas-Marini elements (see for instance [8, 30]). The aim is to compare the accuracy of these inf-sup stable finite elements to approximate the eigenfunctions and eigenvalues of (1.1). It is well known that BDM schemes are more expensive than RT schemes, due to the difference in degrees of freedom between them, which immediately implies the computational costs as first main difference. However, in eigenvalue problems, the orders of convergence and accuracy for the approximation of the spectrum of the solution operator can benefit when using elements that are able to increase their degrees of freedom (see [10, 21, 20, 27] for some papers related to this subject). To make matters precise, in the present work we perform a theoretical and computational analysis for high order mixed methods for the both families of finite elements, where we are interested in their performance in the computation of the spectrum, namely, the accuracy, computational cost and order of convergence.

The paper is organized as follows: in Section 2 we introduce the Stokes eigenvalue problem, for two and three dimensions, together with the pseudostress tensor. With suitable Hilbert spaces we derive a variational formulation for (1.1) where the main

unknowns are the pseudostress, the velocity and the pressure. We introduce the corresponding solution operators and present an additional regularity result for the eigenfunctions. Finally, a spectral characterization is deduced. Section 3 is the core of our paper, where we introduce the finite element schemes of our analysis. We prove the stability for the discrete eigenvalue problem. Also, we introduce the discrete solution operator. In Section 4 we perform the spectral analysis, where convergence and error estimates for the eigenfunctions and eigenvalues are proved. Finally, in Section 5 we report a series of numerical tests where we confirm our theoretical results, together with a comparison between the mixed schemes of our paper.

We end this section with some of the notations that we will use below. Given any Hilbert space X, let X^2 and $\mathbb{X}$ denote, respectively, the space of vectors and tensors with entries in X. In particular, $\mathbb{I}$ is the identity matrix of $\mathbb{R}^{n\times n}$, and $\mathbf{0}$ denotes a generic null vector or tensor. Given $\boldsymbol{\tau} := (\tau_{ij})$ and $\boldsymbol{\sigma} := (\sigma_{ij}) \in \mathbb{R}^{n\times n}$, we define, as usual, the transpose tensor $\boldsymbol{\tau}^{\mathtt{t}} := (\tau_{ji})$, the trace $\mathrm{tr}\,\boldsymbol{\tau} := \sum_{i=1}^n \tau_{ii}$, the deviatoric tensor $\boldsymbol{\tau}^{\mathtt{d}} := \boldsymbol{\tau} - \frac{1}{n}(\mathrm{tr}\,\boldsymbol{\tau})\,\mathbb{I}$, and the tensor inner product $\boldsymbol{\tau} : \boldsymbol{\sigma} := \sum_{i,j=1}^n \tau_{ij}\sigma_{ij}$.

Let Ω be a polygonal Lipschitz bounded domain of $\mathbb{R}^n$ with boundary $\partial\Omega$. For $s \geq 0$, $\|\cdot\|_{s,\Omega}$ stands indistinctly for the norm of the Hilbertian Sobolev spaces $\mathrm{H}^s(\Omega)$, $\mathrm{H}^s(\Omega)^n$ or $\mathbb{H}^s(\Omega)$ for scalar, vectorial and tensorial fields, respectively, with the convention $\mathrm{H}^0(\Omega) := \mathrm{L}^2(\Omega)$, $[\mathrm{H}^0(\Omega)]^n = [\mathrm{L}^2(\Omega)]^n$ and $\mathbb{H}^0(\Omega) := \mathbb{L}^2(\Omega)$. We also define for $s \geq 0$ the Hilbert space $\mathbb{H}^s(\mathbf{div};\Omega) := \{\boldsymbol{\tau} \in \mathbb{H}^s(\Omega) : \ \mathbf{div}\,\boldsymbol{\tau} \in [\mathrm{H}^s(\Omega)]^n\}$, whose norm is given by $\|\boldsymbol{\tau}\|^2_{\mathbf{div},\Omega} := \|\boldsymbol{\tau}\|^2_{s,\Omega} + \|\mathbf{div}\,\boldsymbol{\tau}\|^2_{s,\Omega}$.

The relation $\mathtt{a} \lesssim \mathtt{b}$ indicates that $\mathtt{a} \leq C\mathtt{b}$, with a positive constant C which is independent of $\mathtt{a}$, $\mathtt{b}$ and the mesh size h, which will be introduced in Section 3.

2. The model problem. Let $\Omega = \mathbb{R}^n$, where $n \in \{2,3\}$ represents the dimension, be a bounded simply connected polygonal domain with boundary $\partial\Omega$. We introduce the pseudostress tensor $\boldsymbol{\sigma} := 2\mu\nabla\boldsymbol{u} - p\mathbb{I}$. Hence, system (1.1) is rewritten as follows

$$\left\{\begin{array}{rcll} \mathbf{div}\,\boldsymbol{\sigma} & = & -\lambda\boldsymbol{u} & \text{in}\,\Omega, \\ \boldsymbol{\sigma} - 2\mu\nabla\boldsymbol{u} + p\mathbb{I} & = & \mathbf{0} & \text{in}\,\Omega, \\ p + \dfrac{1}{n}\,\mathrm{tr}(\boldsymbol{\sigma}) & = & 0 & \text{in}\,\Omega, \\ \boldsymbol{u} & = & \mathbf{0} & \text{on}\,\partial\Omega. \end{array}\right. \tag{2.1}$$

See [15] for details related to the derivation of this system. For the analysis of problem (2.1), we are interested in the following variational formulation: Find $\lambda \in \mathbb{R}$ and the triplet $\mathbf{0} \neq (\boldsymbol{\sigma}, p, \boldsymbol{u}) \in \mathbb{H}(\mathbf{div},\Omega) \times \mathrm{L}^2(\Omega) \times [\mathrm{L}^2(\Omega)]^n$ such that

$$\frac{1}{2\mu}\int_\Omega \boldsymbol{\sigma}^{\mathtt{d}} : \boldsymbol{\tau}^{\mathtt{d}} + \frac{n}{2\mu}\int_\Omega \left(p + \frac{1}{n}\,\mathrm{tr}(\boldsymbol{\sigma})\right)\left(q + \frac{1}{n}\,\mathrm{tr}(\boldsymbol{\tau})\right) + \int_\Omega \boldsymbol{u}\cdot\mathbf{div}\,\boldsymbol{\tau} = 0, \tag{2.2}$$

$$\int_\Omega \boldsymbol{v}\cdot\mathbf{div}\,\boldsymbol{\sigma} = -\lambda(\boldsymbol{u},\boldsymbol{v}), \tag{2.3}$$

for all $(\boldsymbol{\tau}, q, \boldsymbol{v}) \in \mathbb{H}(\mathbf{div},\Omega) \times \mathrm{L}^2(\Omega) \times [\mathrm{L}^2(\Omega)]^n$.

It is important to remark that the only eigenfunction in problem (2.2)–(2.3) is the velocity field $\boldsymbol{u}$, and hence the corresponding solution operator is defined only on this unknown (see (2.9) and (2.14) below). This implies that our eigenvalue problem can be defined as follows: Find $(\lambda, \boldsymbol{u}) \in \mathbb{R} \times [\mathrm{L}^2(\Omega)]^n$, with $\boldsymbol{u} \neq \mathbf{0}$ such that there exist $(\boldsymbol{\sigma}, p) \in \mathbb{H}(\mathbf{div},\Omega) \times \mathrm{L}^2(\Omega)$ satisfying (2.2)–(2.3).

For our analysis, the decomposition $\mathbb{H}(\mathbf{div},\Omega) = \mathbb{H}_0 \oplus \mathbb{R}\mathbb{I}$ will be useful (see [15,

Section 2]), where

$$\mathbb{H}_0 := \left\{ \boldsymbol{\tau} \in \mathbb{H}(\mathbf{div}, \Omega) \ : \ \int_\Omega \mathrm{tr}(\boldsymbol{\tau}) = 0 \right\}.$$

In order to simplify the presentation of the material, we define $\mathbb{H} := \mathbb{H}_0 \times \mathrm{L}^2(\Omega)$ and $\mathbf{Q}^{\boldsymbol{u}} := [\mathrm{L}^2(\Omega)]^n$. The bilinear forms $a : \mathbb{H} \times \mathbb{H} \to \mathbb{R}$ and $b : \mathbb{H}(\mathbf{div}, \Omega) \times \mathbf{Q}^{\boldsymbol{u}} \to \mathbb{R}$ are defined as follows:

$$a((\boldsymbol{\xi}, r), (\boldsymbol{\tau}, q)) := \frac{1}{2\mu} \int_\Omega \boldsymbol{\xi}^{\mathtt{d}} : \boldsymbol{\tau}^{\mathtt{d}} + \frac{\gamma}{\mu} \left(p + \frac{1}{n} \mathrm{tr}(\boldsymbol{\xi}) \right) \left(q + \frac{1}{n} \mathrm{tr}(\boldsymbol{\tau}) \right),$$

$$b(\boldsymbol{\xi}, \boldsymbol{v}) := \int_\Omega \boldsymbol{v} \cdot \mathbf{div}\, \boldsymbol{\xi}.$$

According to [15, Lemma 2.2], we have that any solution of problem (2.2)–(2.3) with $\boldsymbol{\sigma} \in \mathbb{H}_0$ is also solution of

$$a((\boldsymbol{\sigma}, p), (\boldsymbol{\tau}, q)) + b(\boldsymbol{\tau}, \boldsymbol{u}) = 0 \qquad \forall (\boldsymbol{\tau}, q) \in \mathbb{H}, \tag{2.4}$$

$$b(\boldsymbol{\sigma}, \boldsymbol{v}) = -\lambda(\boldsymbol{u}, \boldsymbol{v}) \quad \forall \boldsymbol{v} \in \mathbf{Q}^{\boldsymbol{u}}, \tag{2.5}$$

with $\gamma = 1$ if $n = 2$ and $\gamma = 3/2$ if $n = 3$, whereas any solution of (2.4)–(2.5) is also a solution of problem (2.2)–(2.3).

It is possible to consider an alternative reduced formulation for our problem (2.4)–(2.5), which only depends on the stress tensor and the velocity.

With the space $\mathbb{H}_0$ at hand, we consider the following problem: find $\lambda \in \mathbb{R}$ and $\mathbf{0} \neq (\boldsymbol{\sigma}, \boldsymbol{u}) \in \mathbb{H}_0 \times \mathbf{Q}^{\boldsymbol{u}}$ such that

$$a_0(\boldsymbol{\sigma}, \boldsymbol{\tau}) + b(\boldsymbol{\tau}, \boldsymbol{u}) = 0 \qquad \forall \boldsymbol{\tau} \in \mathbb{H}_0, \tag{2.6}$$

$$b(\boldsymbol{\sigma}, \boldsymbol{v}) = -\lambda(\boldsymbol{u}, \boldsymbol{v}) \quad \forall \boldsymbol{v} \in \mathbf{Q}^{\boldsymbol{u}}, \tag{2.7}$$

where $a_0 : \mathbb{H}_0 \times \mathbb{H}_0 \to \mathbb{R}$ is a bounded bilinear form defined by

$$a_0(\boldsymbol{\xi}, \boldsymbol{\tau}) := \frac{1}{2\mu} \int_\Omega \boldsymbol{\xi}^{\mathtt{d}} : \boldsymbol{\tau}^{\mathtt{d}} \quad \forall (\boldsymbol{\xi}, \boldsymbol{\tau}) \in \mathbb{H}_0 \times \mathbb{H}_0.$$

We remark that the pressure can be recovered with the third equation of system (2.1).

Remark 2.1. It is easy to check that $(\lambda, \boldsymbol{\sigma}, p, \boldsymbol{u}) \in \mathbb{R} \times \mathbb{H} \times \mathbf{Q}$ is a solution of problem (2.4)–(2.5) if and only if $(\lambda, \boldsymbol{\sigma}, \boldsymbol{u}) \in \mathbb{R} \times \mathbb{H}_0 \times \mathbf{Q}$ is a solution of problem (2.6)–(2.7), together with the third equation of system (2.1) (see [15, Lemma 2.3]).

For the analysis of the mixed problem (2.6)–(2.7) we invoke the following result (see [5, Ch. 9, Proposition 9.1.1])

$$\|\boldsymbol{\tau}\|_{0,\Omega}^2 \lesssim \|\boldsymbol{\tau}^{\mathtt{d}}\|_{0,\Omega}^2 + \|\mathbf{div}\, \boldsymbol{\tau}\|_{0,\Omega}^2 \quad \forall \boldsymbol{\tau} \in \mathbb{H}_0. \tag{2.8}$$

Let us introduce the kernel of the operator induced by $b(\cdot, \cdot)$

$$\mathcal{V} := \{ \boldsymbol{\tau} \in \mathbb{H}_0 \ : \ b(\boldsymbol{\tau}, \boldsymbol{v}) = 0 \ \ \forall \boldsymbol{v} \in \mathbf{Q} \} = \{ \boldsymbol{\tau} \in \mathbb{H}_0 \ : \ \mathbf{div}\, \boldsymbol{\tau} = \mathbf{0} \}.$$

With the aid of (2.8) it is easy to check that $a_0(\cdot, \cdot)$ is coercive in $\mathcal{V}$ (see [15, Subsection 2.3]). On the other hand, there exists a positive constant β such that the following inf-sup condition for $b(\cdot, \cdot)$ holds (see [15, Theorem 2.1])

$$\sup_{\mathbf{0}\neq\boldsymbol{\tau}\in\mathbb{H}_0}\frac{b(\boldsymbol{\tau},\boldsymbol{v})}{\|\boldsymbol{\tau}\|_{\mathbf{div},\Omega}}\geq\beta\|\boldsymbol{v}\|_{0,\Omega}\quad\forall\boldsymbol{v}\in\mathbf{Q}^{\boldsymbol{u}}.$$

With these results at hand, we are in position to introduce the solution operator

$$\boldsymbol{T}:\mathbf{Q}^{\boldsymbol{u}}\to\mathbf{Q}^{\boldsymbol{u}},\qquad\boldsymbol{f}\mapsto\boldsymbol{T}\boldsymbol{f}:=\widehat{\boldsymbol{u}},\tag{2.9}$$

where the pair $(\widehat{\boldsymbol{\sigma}},\widehat{\boldsymbol{u}})\in\mathbb{H}_0\times\mathbf{Q}^{\boldsymbol{u}}$ is the solution of the following well posed source problem

$$a_0(\widehat{\boldsymbol{\sigma}},\boldsymbol{\tau})+b(\boldsymbol{\tau},\widehat{\boldsymbol{u}})=0\qquad\forall\boldsymbol{\tau}\in\mathbb{H}_0,\tag{2.10}$$

$$b(\widehat{\boldsymbol{\sigma}},\boldsymbol{v})=-(\boldsymbol{f},\boldsymbol{v})\quad\forall\boldsymbol{v}\in\mathbf{Q}^{\boldsymbol{u}},\tag{2.11}$$

implying that $\boldsymbol{T}$ is well defined due to the Babuŝka-Brezzi theory. Moreover, we have the following estimate

$$\|\widehat{\boldsymbol{\sigma}}\|_{\mathbf{div},\Omega}+\|\widehat{\boldsymbol{u}}\|_{0,\Omega}\lesssim\|\boldsymbol{f}\|_{0,\Omega}.\tag{2.12}$$

Moreover, it is easy to check that $\boldsymbol{T}$ is self-adjoint respect to the $[\mathrm{L}^2(\Omega)]^n$ inner product. Indeed, given $\widehat{\boldsymbol{f}},\widetilde{\boldsymbol{f}}\in\mathbf{Q}^{\boldsymbol{u}}$, let $(\widehat{\boldsymbol{\sigma}},\widehat{\boldsymbol{u}})\in\mathbb{H}_0\times\mathbf{Q}^{\boldsymbol{u}}$ and $(\widetilde{\boldsymbol{\sigma}},\widetilde{\boldsymbol{u}})\in\mathbb{H}_0\times\mathbf{Q}^{\boldsymbol{u}}$ be the solutions to problem (2.10)–(2.11) with right hand sides $\widehat{\boldsymbol{f}}$ and $\widetilde{\boldsymbol{f}}$, respectively. Assume that $\boldsymbol{T}\widehat{\boldsymbol{f}}=\widehat{\boldsymbol{u}}$ and $\boldsymbol{T}\widetilde{\boldsymbol{f}}=\widetilde{\boldsymbol{u}}$. From the symmetry of $a_0(\cdot,\cdot)$ and $(\cdot,\cdot)_{0,\Omega}$ we have that

$$(\widehat{\boldsymbol{f}},\boldsymbol{T}\widetilde{\boldsymbol{f}})_{0,\Omega}=(\widehat{\boldsymbol{f}},\widetilde{\boldsymbol{u}})_{0,\Omega}=-b(\widehat{\boldsymbol{\sigma}},\widetilde{\boldsymbol{u}})=-b(\widetilde{\boldsymbol{\sigma}},\widehat{\boldsymbol{u}})=(\widetilde{\boldsymbol{f}},\widehat{\boldsymbol{u}})_{0,\Omega}=(\boldsymbol{T}\widehat{\boldsymbol{f}},\widetilde{\boldsymbol{f}})_{0,\Omega}.$$

We observe that $(\lambda,(\boldsymbol{\sigma},\boldsymbol{u}))\in\mathbb{R}\times\mathbb{H}_0\times\mathbf{Q}^{\boldsymbol{u}}$ solves (2.6)–(2.7) if and only if $(\kappa,\boldsymbol{u})$ is an eigenpair of $\boldsymbol{T}$, i.e. $\boldsymbol{T}\boldsymbol{u}=\kappa\boldsymbol{u}$ with $\kappa:=1/\lambda$.

From [13, 32] we have the following regularity result for the Stokes spectral problem.

THEOREM 2.2. *If* $(\lambda,\boldsymbol{u},p)\in[\mathrm{H}^1_0(\Omega)]^n\times\mathrm{L}^2_0(\Omega)\times\mathbb{R}$ *solves* (1.1)*, there exists* $s>0$ *such that* $\boldsymbol{u}\in[\mathrm{H}^{1+s}(\Omega)]^n$ *and* $p\in\mathrm{H}^s(\Omega)$.

We observe that Theorem 2.2, together with the first and second equations of (2.1) reveal that $\mathbf{div}\,\boldsymbol{\sigma}\in[\mathrm{H}^{1+s}(\Omega)]^n$ and $\boldsymbol{\sigma}\in[\mathrm{H}^s(\Omega)]^n$, respectively. This additional regularity for the pseudotress tensor is a key ingredient for the numerical approximation.

Remark 2.3. Note that the estimate

$$\|\widehat{\boldsymbol{\sigma}}\|_{s,\Omega}+\|\widehat{\boldsymbol{u}}\|_{1+s,\Omega}\lesssim\|\boldsymbol{f}\|_{0,\Omega}\tag{2.13}$$

holds. Hence, the operator $\boldsymbol{T}$ is compact. Moreover, the spectrum of $\boldsymbol{T}$ satisfies $\mathrm{sp}(\boldsymbol{T})=\{0\}\cup\{\mu_k\}_{k\in\mathbb{N}}$, where $\{\mu_k\}_{k\in\mathbb{N}}\in(0,1)$ is a sequence of real positive eigenvalues which converges to zero, repeated according their respective multiplicities.

We have from Remark 2.1 that problems (2.4)–(2.5) and (2.6)–(2.7) are equivalent. However, the finite element discretizations for these problems are not equivalent (cf. Section 3). Hence, to obtain error estimates for our methods, we need to consider an additional solution operator associated with the problem (2.4)–(2.5).

Now, let $\widetilde{\boldsymbol{T}}$ be the solution operator defined by

$$\widetilde{\boldsymbol{T}} : \mathbf{Q}^{\boldsymbol{u}} \to \mathbf{Q}^{\boldsymbol{u}}, \qquad \boldsymbol{f} \mapsto \widetilde{\boldsymbol{T}}\widetilde{\boldsymbol{f}} := \widetilde{\boldsymbol{u}}, \tag{2.14}$$

where $(\widetilde{\boldsymbol{\sigma}}, \widetilde{p}, \widetilde{\boldsymbol{u}}) \in \mathbb{H} \times \mathbf{Q}^{\boldsymbol{u}}$ is the solution of the following source problem

$$\begin{aligned} a((\widetilde{\boldsymbol{\sigma}}, \widetilde{p}), (\boldsymbol{\tau}, q)) + b(\boldsymbol{\tau}, \widetilde{\boldsymbol{u}}) &= 0 \qquad \forall (\boldsymbol{\tau}, q) \in \mathbb{H}, \\ b(\widetilde{\boldsymbol{\sigma}}, \boldsymbol{v}) &= -(\widetilde{\boldsymbol{f}}, \boldsymbol{v}) \quad \forall \boldsymbol{v} \in \mathbf{Q}^{\boldsymbol{u}}. \end{aligned}$$

Thanks to Remark 2.1 and the fact that the operator $\boldsymbol{T}$ is well-defined, we have that also that $\widetilde{\boldsymbol{T}}$ is well defined (see [15, Theorem 2.2]).

Moreover, it is easy to check that $\widetilde{\boldsymbol{T}}$ is self-adjoint respect the $[\mathrm{L}^2(\Omega)]^n$- inner product and that the pair $(\lambda, (\boldsymbol{\sigma}, p, \boldsymbol{u})) \in \mathbb{R} \times \mathbb{H} \times \mathbf{Q}^{\boldsymbol{u}}$ solves (2.4)–(2.5) if and only if $(\kappa, \boldsymbol{u})$ is an eigenpair of $\widetilde{\boldsymbol{T}}$. Hence, $\widetilde{\boldsymbol{T}}$ is compact and $\mathrm{sp}(\widetilde{\boldsymbol{T}}) = \mathrm{sp}(\boldsymbol{T}) = \{0\} \cup \{\mu_k\}_{k \in \mathbb{N}}$.

3. The mixed finite element method. The present section deals with the finite element approximation for the eigenvalue problem. To do this task, we begin by introducing a regular family of triangulations of Ω denoted by $\{\mathcal{T}_h\}_{h>0}$. Let h_T the diameter of a triangle T of the triangulation and let us define $h := \max\{h_T : T \in \mathcal{T}_h\}$.

Given an integer $\ell \geq 0$ and a subset D of $\mathbb{R}^n$, we denote by $\mathbb{P}_\ell(D)$ the space of polynomials of degree at most ℓ defined in D.

3.1. The finite element spaces. In our study, we consider two numerical schemes that only differ in the space that approximates the pseudostress. Hence, we only refer to $\mathbb{H}_h^{\boldsymbol{\sigma}}$ as the finite element space related to the approximation of $\boldsymbol{\sigma}$. For the velocity field, we consider the space $\mathbf{Q}_h^{\boldsymbol{u}}$ and for the pressure Q_h^p. In what follows, we specify each of these finite dimensional spaces.

For $k \geq 0$ we define the local Raviart-Thomas space of order k as follows (see [5])

$$\mathbb{RT}_k(T) = [\mathbb{P}_k(T)]^n \oplus \mathbb{P}_k(T)\boldsymbol{x},$$

where if $\mathtt{t}$ denotes the transpose operator, $\boldsymbol{x}^{\mathtt{t}}$ represents a generic vector of $\mathbb{R}^n$. Hence, the global Raviart-Thomas space is defined by

$$\mathbb{RT}_k(\mathcal{T}_h) := \{\boldsymbol{\tau} \in \mathbb{H}(\mathbf{div}, \Omega) : \boldsymbol{\tau}|_T^{\mathtt{t}} \in \mathbb{RT}_k(T), \ \forall T \in \mathcal{T}_h\}.$$

More precisely, in the definition above $\boldsymbol{\tau}|_T^{\mathtt{t}}$ must be understood as $(\tau_{i1}, \tau_{i2})^{\mathtt{t}} \in \mathbb{RT}_k(T)$ for all $i \in \{1, 2\}$ when $n = 2$, and $(\tau_{j1}, \tau_{j2}, \tau_{j3})^{\mathtt{t}} \in \mathbb{RT}_k(T)$ for all $j \in \{1, 2, 3\}$ when $n = 3$.

On the other hand, we define the space of piecewise polynomials of degree at most k

$$\mathbb{P}_k(\mathcal{T}_h) := \{v \in \mathrm{L}^2(\Omega) : v|_T \in \mathbb{P}_k(T) \ \forall T \in \mathcal{T}_h\}.$$

In addition, we introduce the Brezzi-Douglas-Marini finite element space [8],

$$\mathbb{BDM}_k := [\mathbb{P}_k(\mathcal{T}_h)]^n \cap \mathbb{H} \text{ with } k \geq 1.$$

It is well known from the literature that $\mathbb{RT}_{k-1} \subset \mathbb{BDM}_k \subset \mathbb{RT}_k$ for all $k \geq 1$ (see [5, Section 2]). Moreover, the number of degrees of freedom per edge is the same for both finite elements, however, the number of internal degrees of freedom of Brezzi-Douglas-Marini ($\mathbb{BDM}_k$) elements is less than that of standard finite elements

of the same order such as Raviart-Thomas ($\mathbb{RT}_k$). A count of the internal degrees of freedom for $n = 2$ gives

$$\mathbb{BDM}_k : 2(k-1)(k+1), \qquad \mathbb{RT}_k : 2k(k+1),$$

and for $n = 3$

$$\mathbb{BDM}_k : \frac{3}{2}(k-1)(k+1)(k+2), \qquad \mathbb{RT}_k : \frac{3}{2}k(k+1)(k+2).$$

3.2. Approximation errors. In the following, some approximation results for discrete spaces are presented. To make matters precise, since we consider two spaces to approximate the pseudostress tensor, we need to introduce suitable interpolators for each finite element space, namely, Raviart-Thomas and BDM spaces. We begin with the classical approximation property for piecewise polynomials (see [5]). Let $\mathcal{R}_h : [\mathrm{L}^2(\Omega)]^n \to [\mathbb{P}_k(\mathcal{T}_h)]^n$. The following estimate holds

$$\|\boldsymbol{v} - \mathcal{R}_h\boldsymbol{v}\|_{0,\Omega} \lesssim h^{\min\{t,k+1\}}\|\boldsymbol{v}\|_{t,\Omega} \qquad \forall t \in [\mathrm{H}^t(\Omega)]^n \cap [\mathrm{L}^2(\Omega)]^n. \tag{3.1}$$

For the Raviart-Thomas spaces, we have the following approximation results: let $\boldsymbol{\Pi}_h^{\mathbb{RT}} : [\mathbb{H}^t(\Omega)]^{n\times n} \to \mathbb{RT}_k$ be the tensorial version of the Raviart-Thomas interpolation operator , which satisfies the following classical error estimate, see [9, 31],

$$\|\boldsymbol{\tau} - \boldsymbol{\Pi}_h^{\mathbb{RT}}\boldsymbol{\tau}\|_{0,\Omega} \lesssim h^{\min\{t,k+1\}}\|\boldsymbol{\tau}\|_{t,\Omega} \qquad \forall \boldsymbol{\tau} \in [\mathbb{H}^t(\Omega)]^{n\times n}, \quad t \geq 1. \tag{3.2}$$

Also, thanks to the commuting diagram, if $\operatorname{div}\boldsymbol{\tau} \in [\mathbf{H}^r(\Omega)]^n$ with $r \geq 0$ we have the following result

$$\|\mathbf{div}(\boldsymbol{\tau} - \boldsymbol{\Pi}_h^{\mathbb{RT}}\boldsymbol{\tau})\|_{0,\Omega} = \|\mathbf{div}\,\boldsymbol{\tau} - \mathcal{R}_h\,\mathbf{div}\,\boldsymbol{\tau}\|_{0,\Omega} \lesssim h^{\min\{r,k+1\}}\|\mathbf{div}\,\boldsymbol{\tau}\|_{r,\Omega}. \tag{3.3}$$

Moreover, $\boldsymbol{\Pi}_h^{\mathbb{RT}}$ can also be defined as $\boldsymbol{\Pi}_h^{\mathbb{RT}} : [\mathbb{H}^t(\Omega)]^{n\times n} \cap \mathbb{H}(\mathbf{div},\Omega) \to \mathbb{RT}_k$ for all $t \in (0,1]$, and we have the following estimate

$$\|\boldsymbol{\tau} - \boldsymbol{\Pi}_h^{\mathbb{RT}}\boldsymbol{\tau}\|_{0,\Omega} \lesssim h^t(\|\boldsymbol{\tau}\|_{t,\Omega} + \|\mathbf{div}\,\boldsymbol{\tau}\|_{0,\Omega}) \quad \forall \boldsymbol{\tau} \in [\mathbb{H}^t(\Omega)]^{n\times n} \cap \mathbb{H}(\mathbf{div},\Omega) \quad t \in (0,1]. \tag{3.4}$$

For the BDM spaces, we have the following properties: let $\ell \geq 1$ and let $\boldsymbol{\Pi}_h^{\mathbb{BDM}} : [\mathbb{H}^t(\Omega)]^{n\times n} \to \mathbb{BDM}_\ell$ be the tensorial version of the BDM-interpolation operator, which satisfies the following classical error estimate, see [18, Theorem 3.16],

$$\|\boldsymbol{\tau} - \boldsymbol{\Pi}_h^{\mathbb{BDM}}\boldsymbol{\tau}\|_{0,\Omega} \lesssim h^{\min\{t,\ell+1\}}\|\boldsymbol{\tau}\|_{t,\Omega} \qquad \forall \boldsymbol{\tau} \in [\mathbb{H}^t(\Omega)]^{n\times n}, \quad t > 1/2. \tag{3.5}$$

Moreover, for less regular tensorial fields we have the following estimate

$$\|\boldsymbol{\tau} - \boldsymbol{\Pi}_h^{\mathbb{BDM}}\boldsymbol{\tau}\|_{0,\Omega} \lesssim h^t(\|\boldsymbol{\tau}\|_{t,\Omega} + \|\boldsymbol{\tau}\|_{\mathbf{div},\Omega}) \;\; \forall \boldsymbol{\tau} \in [\mathbb{H}^t(\Omega)]^{n\times n} \cap \mathbb{H}(\mathbf{div},\Omega), \;\; t \in (0,1/2]. \tag{3.6}$$

The following commuting diagram property holds true

$$\|\mathbf{div}(\boldsymbol{\tau} - \boldsymbol{\Pi}_h^{\mathbb{BDM}}\boldsymbol{\tau})\|_{0,\Omega} = \|\mathbf{div}\,\boldsymbol{\tau} - \mathcal{R}_h\,\mathbf{div}\,\boldsymbol{\tau}\|_{0,\Omega} \lesssim h^{\min\{t,\ell\}}\|\mathbf{div}\,\boldsymbol{\tau}\|_{t,\Omega}, \tag{3.7}$$

for $\mathbf{div}\,\boldsymbol{\tau} \in [\mathrm{H}^t(\Omega)]^n$ and $\mathcal{R}_h$ being the $[\mathrm{L}^2(\Omega)]^n$-orthogonal projection onto $[\mathbb{P}_{\ell-1}(\mathcal{T}_h)]^n$.

We conclude this section by introducing the following notations

$$\mathbb{H}_{0,h}^{\boldsymbol{\sigma}} := \left\{ \boldsymbol{\tau} \in \mathbb{H}_h^{\boldsymbol{\sigma}} \;:\; \int_\Omega \operatorname{tr}(\boldsymbol{\tau}) = 0 \right\},$$

where $\mathbb{H}_h^{\boldsymbol{\sigma}} \in \{\mathbb{RT}_k, \mathbb{BDM}_{k+1}\}$. Also, we define $Q_h^p := \mathbb{P}_k(\mathcal{T}_h)$, $\mathbf{Q}_h^{\boldsymbol{u}} := [\mathbb{P}_k(\mathcal{T}_h)]^n$ and $\mathbb{H}_h := \mathbb{H}_h^{\boldsymbol{\sigma}} \times Q_h^p$.

Therefore, as a consequence of (3.1)–(3.7), we have the following approximation properties for $k \geq 0$: For each $t > 0$ and for each $\boldsymbol{\tau} \in \mathbb{H}^t(\Omega) \cap \mathbb{H}_0$ with $\mathbf{div}\, \boldsymbol{\tau} \in [\mathrm{H}^t(\Omega)]^n$ there exists $\boldsymbol{\tau}_h \in \mathbb{H}_0^\sigma$ such that

$$\|\boldsymbol{\tau} - \boldsymbol{\tau}_h\|_{\mathbf{div},\Omega} \lesssim h^{\min\{t,k+1\}} \left(\|\boldsymbol{\tau}\|_{t,\Omega} + \|\,\mathbf{div}\,\boldsymbol{\tau}\|_{t,\Omega}\right). \tag{3.8}$$

For $q \in Q^p$ there exists $q_h \in Q_h^p$ such that

$$\|q - q_h\|_{0,\Omega} \lesssim h^{\min\{t,k+1\}} \|q\|_{t,\Omega}. \tag{3.9}$$

For $\boldsymbol{v} \in [\mathrm{H}^t(\Omega)]^n$ there exists $\boldsymbol{v}_h \in \mathbf{Q}_h^{\boldsymbol{u}}$ such that

$$\|\boldsymbol{v} - \boldsymbol{v}_h\|_{0,\Omega} \lesssim h^{\min\{t,k+1\}} \|\boldsymbol{v}\|_{t,\Omega}. \tag{3.10}$$

3.3. Discrete eigenvalue problems. As we claim in Section 2, discrete counterparts of problems (2.4)–(2.5) and (2.6)–(2.7) are not equivalent (see [15, Lemma 3.1] for further details). Hence, we need to analyze each discrete eigenvalue problem separately.

With the discrete spaces defined above, we are in position to introduce the discretization of problem (2.4)–(2.5): Find $\lambda_h \in \mathbb{R}$ and $\mathbf{0} \neq (\boldsymbol{\sigma}_h, p_h, \boldsymbol{u}_h) \in \mathbb{H}_h \times \mathbf{Q}_h^{\boldsymbol{u}}$ such that

$$a((\boldsymbol{\sigma}_h, p_h), (\boldsymbol{\tau}_h, q_h)) + b(\boldsymbol{\tau}_h, \boldsymbol{u}_h) = 0 \qquad \forall (\boldsymbol{\tau}_h, q_h) \in \mathbb{H}_h, \tag{3.11}$$

$$b(\boldsymbol{\sigma}_h, \boldsymbol{v}_h) = -\lambda_h (\boldsymbol{u}_h, \boldsymbol{v}_h) \quad \forall \boldsymbol{v}_h \in \mathbf{Q}_h^{\boldsymbol{u}}. \tag{3.12}$$

Similarly as in the continuous case, it is possible to consider a reduced formulation for the discrete eigenvalue problem. These reduced discrete problem reads as follows: find $\lambda_h \in \mathbb{R}$ and $\mathbf{0} \neq (\boldsymbol{\sigma}_h, \boldsymbol{u}_h) \in \mathbb{H}_{0,h}^{\boldsymbol{\sigma}} \times \mathbf{Q}_h^{\boldsymbol{u}}$ such that

$$a_0(\boldsymbol{\sigma}_h, \boldsymbol{\tau}_h) + b(\boldsymbol{\tau}_h, \boldsymbol{u}_h) = 0 \qquad \forall \boldsymbol{\tau}_h \in \mathbb{H}_{0,h}^{\boldsymbol{\sigma}}, \tag{3.13}$$

$$b(\boldsymbol{\sigma}_h, \boldsymbol{v}_h) = -\lambda (\boldsymbol{u}_h, \boldsymbol{v}_h) \quad \forall \boldsymbol{v}_h \in \mathbf{Q}_h^{\boldsymbol{u}}. \tag{3.14}$$

It has been proved in [15, Lemma 3.2] that there exists a positive constant β, independent of h, such that the following inf-sup condition holds

$$\sup_{\mathbf{0} \neq \boldsymbol{\tau}_h \in \mathbb{H}_{0,h}^{\boldsymbol{\sigma}}} \frac{b(\boldsymbol{\tau}_h, \boldsymbol{v}_h)}{\|\boldsymbol{\tau}_h\|_{\mathbf{div},\Omega}} \geq \beta \|\boldsymbol{v}_h\|_{0,\Omega} \quad \forall \boldsymbol{v}_h \in \mathbf{Q}_h^{\boldsymbol{u}}. \tag{3.15}$$

On the other hand, the discrete kernel of $b(\cdot,\cdot)$ (namely, the kernel of the operator induced by $b(\cdot,\cdot)$) is defined by

$$\mathcal{V}_h := \{\boldsymbol{\tau} \in \mathbb{H}_{0,h}^{\sigma} \,:\, b(\boldsymbol{\tau}, \boldsymbol{v}) = 0 \ \forall \boldsymbol{v} \in \mathbf{Q}_h^{\boldsymbol{u}}\} = \{\boldsymbol{\tau} \in \mathbb{H}_{0,h}^{\sigma} \,:\, \mathbf{div}\,\boldsymbol{\tau} = \mathbf{0} \ \text{ in } \Omega\}.$$

In [15, Theorem 3.1] the authors have stated that $a_0(\cdot,\cdot)$ is coercive in $\mathcal{V}_h$ and that $b(\cdot,\cdot)$ satisfies the corresponding discrete inf-sup condition.

With these ingredients at hand, we are in position to introduce the discrete solution operator associated to (3.13)–(3.14)

$$\boldsymbol{T}_h : \mathbf{Q}^{\boldsymbol{u}} \to \mathbf{Q}_h^{\boldsymbol{u}}, \qquad \boldsymbol{f} \mapsto \boldsymbol{T}_h \boldsymbol{f} := \widehat{\boldsymbol{u}}_h,$$

where $(\widehat{\boldsymbol{\sigma}}_h, \widehat{\boldsymbol{u}}_h) \in \mathbb{H}^{\boldsymbol{\sigma}}_{0,h} \times \mathbf{Q}^{\boldsymbol{u}}_h$ is the solution of the following source problem

$$a_0(\widehat{\boldsymbol{\sigma}}_h, \boldsymbol{\tau}_h) + b(\boldsymbol{\tau}_h, \widehat{\boldsymbol{u}}_h) = 0 \qquad \forall \boldsymbol{\tau}_h \in \mathbb{H}^{\sigma}_{0,h}, \tag{3.16}$$

$$b(\widehat{\boldsymbol{\sigma}}_h, \boldsymbol{v}_h) = -(\boldsymbol{f}, \boldsymbol{v}_h) \quad \forall \boldsymbol{v}_h \in \mathbf{Q}^{\boldsymbol{u}}_h, \tag{3.17}$$

which according to the Babuŝka-Brezzi theory, is well posed (see [5]).

As is stated in [15, Lemma 3.1], a necessary condition for the equivalence between discrete problem (3.11)–(3.12) and problem (3.13)–(3.14) is that $\mathrm{tr}(\mathbb{H}^{\sigma}_{0,h}) \subset Q^p_h$ and, since in this case, this condition does not hold, we need to define the following discrete solution operator $\widetilde{\boldsymbol{T}}_h$ associated with the problem (3.11)–(3.12)

$$\widetilde{\boldsymbol{T}}_h : \mathbf{Q}^{\boldsymbol{u}} \to \mathbf{Q}^{\boldsymbol{u}}_h, \qquad \widetilde{\boldsymbol{f}} \mapsto \widetilde{\boldsymbol{T}}_h \widetilde{\boldsymbol{f}} := \widetilde{\boldsymbol{u}}_h,$$

where the triplet $(\widetilde{\boldsymbol{\sigma}}_h, \widetilde{p}_h, \widetilde{\boldsymbol{u}}_h) \in \mathbb{H}_h \times \mathbf{Q}^{\boldsymbol{u}}_h$ is the solution of the following source problem

$$\begin{aligned} a((\widetilde{\boldsymbol{\sigma}}_h, \widetilde{p}_h), (\boldsymbol{\tau}_h, q_h)) + b(\boldsymbol{\tau}_h, \widetilde{\boldsymbol{u}}_h) &= 0 \qquad \forall (\boldsymbol{\tau}_h, q_h) \in \mathbb{H}_h, \\ b(\widetilde{\boldsymbol{\sigma}}_h, \boldsymbol{v}_h) &= -(\widetilde{\boldsymbol{f}}, \boldsymbol{v}_h) \quad \forall \boldsymbol{v}_h \in \mathbf{Q}^{\boldsymbol{u}}_h. \end{aligned}$$

Observe that [15, Theorem 3.3] guarantees that $\widetilde{\boldsymbol{T}}_h$ is well-defined.

4. Convergence and Error estimates. Since $\boldsymbol{T}$ is compact, under the approach of the classic compact operator theory of [3], the present section is dedicated to derive approximation results related to the continuous and discrete solutions operators, leading to the approximation of the respective spectrums. Once we obtain these results, error estimates for the eigenfunctions and eigenvalues will be proved. We remark that, for both of the numerical schemes considered in our paper, these results are valid.

4.1. Convergence analysis. We begin by analyzing the convergence of $\boldsymbol{T}_h$ to $\boldsymbol{T}$ as h goes to zero. Since our aim is to use the compact operators theory, this convergence is in norm, more precisely, and due to the definition of $\boldsymbol{T}$, in the $\mathrm{L}^2(\Omega)$ norm. This analysis is presented in the following result.

LEMMA 4.1. *Let $\boldsymbol{f} \in \mathbf{Q}^{\boldsymbol{u}}$. If $\boldsymbol{\Pi}_h$ represents the RT-interpolation operator ($\boldsymbol{\Pi}^{\mathbb{RT}}_h$) or the BDM-interpolation operator ($\boldsymbol{\Pi}^{\mathbb{BDM}}_h$), as appropriate, there holds*

$$\|(\boldsymbol{T} - \boldsymbol{T}_h)\boldsymbol{f}\|_{0,\Omega} \lesssim \|\widehat{\boldsymbol{\sigma}} - \boldsymbol{\Pi}_h \widehat{\boldsymbol{\sigma}}\|_{0,\Omega} + \|\widehat{\boldsymbol{u}} - \mathcal{R}_h \widehat{\boldsymbol{u}}\|_{0,\Omega},$$

and

$$\|(\widetilde{\boldsymbol{T}} - \widetilde{\boldsymbol{T}}_h)\boldsymbol{f}\|_{0,\Omega} \lesssim \|\widetilde{\boldsymbol{\sigma}} - \boldsymbol{\Pi}_h \widetilde{\boldsymbol{\sigma}}\|_{0,\Omega} + \|\widetilde{p} - \mathcal{R}_h \widetilde{p}\|_{0,\Omega} + \|\widetilde{\boldsymbol{u}} - \mathcal{R}_h \widetilde{\boldsymbol{u}}\|_{0,\Omega},$$

where the hidden constant are independent of h.

Proof. Let $\boldsymbol{f} \in \mathbf{Q}^{\boldsymbol{u}}$ be such that $\boldsymbol{T}\boldsymbol{f} = \widehat{\boldsymbol{u}}$ and $\boldsymbol{T}_h\boldsymbol{f} = \widehat{\boldsymbol{u}}_h$ where $\widehat{\boldsymbol{u}}$ is the solution of (2.10)–(2.11) and $\widehat{\boldsymbol{u}}_h$ is the solution of (3.16)–(3.17), we have

$$\|(\boldsymbol{T} - \boldsymbol{T}_h)\boldsymbol{f}\|_{0,\Omega} = \|\widehat{\boldsymbol{u}} - \widehat{\boldsymbol{u}}_h\|_{0,\Omega} \leq \|\widehat{\boldsymbol{u}} - \mathcal{R}_h \widehat{\boldsymbol{u}}\|_{0,\Omega} + \|\mathcal{R}_h \widehat{\boldsymbol{u}} - \widehat{\boldsymbol{u}}_h\|_{0,\Omega}. \tag{4.1}$$

Set $\boldsymbol{v}_h := \mathcal{R}_h \widehat{\boldsymbol{u}} - \widehat{\boldsymbol{u}}_h \in \mathbf{Q}^{\boldsymbol{u}}_h$ in (3.15). Then

$$\|\mathcal{R}_h \widehat{\boldsymbol{u}} - \widehat{\boldsymbol{u}}_h\|_{0,\Omega} \leq \frac{1}{\beta} \sup_{\mathbf{0} \neq \boldsymbol{\tau}_h \in \mathbb{H}^{\boldsymbol{\sigma}}_{0,h}} \frac{b(\boldsymbol{\tau}_h, \mathcal{R}_h \widehat{\boldsymbol{u}} - \widehat{\boldsymbol{u}}_h)}{\|\boldsymbol{\tau}_h\|_{\mathbf{div},\Omega}}.$$

Now, the fact that $\boldsymbol{\tau}_h \in \mathbb{H}^{\boldsymbol{\sigma}}_{0,h}$, then $\mathbf{div}(\boldsymbol{\tau}_h) \in \mathbf{Q}^{\boldsymbol{u}}_h$ and using that $\mathcal{R}_h$ is the $\mathrm{L}^2(\Omega)$-orthogonal projector, we have

$$\begin{aligned} b(\boldsymbol{\tau}_h, \mathcal{R}_h\widehat{\boldsymbol{u}} - \widehat{\boldsymbol{u}}_h) &= b(\boldsymbol{\tau}_h, \widehat{\boldsymbol{u}}) - b(\boldsymbol{\tau}_h, \widehat{\boldsymbol{u}}_h) \\ &= a_0(\widehat{\boldsymbol{\sigma}}_h, \boldsymbol{\tau}_h) - a_0(\widehat{\boldsymbol{\sigma}}, \boldsymbol{\tau}_h) \lesssim \|\widehat{\boldsymbol{\sigma}}_h - \widehat{\boldsymbol{\sigma}}\|_{0,\Omega}\|\boldsymbol{\tau}_h\|_{0,\Omega}, \end{aligned}$$

where we have used (2.10) and (3.16). Therefore

$$\|\mathcal{R}^k_h\widehat{\boldsymbol{u}} - \widehat{\boldsymbol{u}}_h\|_{0,\Omega} \lesssim \|\widehat{\boldsymbol{\sigma}}_h - \widehat{\boldsymbol{\sigma}}\|_{0,\Omega}. \tag{4.2}$$

The following step is to bound $\|\widehat{\boldsymbol{\sigma}} - \widehat{\boldsymbol{\sigma}}_h\|_{0,\Omega}$. From the triangle inequality we have

$$\|\widehat{\boldsymbol{\sigma}} - \widehat{\boldsymbol{\sigma}}_h\|_{0,\Omega} \leq \|\widehat{\boldsymbol{\sigma}} - \boldsymbol{\Pi}_h\widehat{\boldsymbol{\sigma}}\|_{0,\Omega} + \|\boldsymbol{\Pi}_h\widehat{\boldsymbol{\sigma}} - \widehat{\boldsymbol{\sigma}}_h\|_{0,\Omega}, \tag{4.3}$$

where $\boldsymbol{\Pi}_h$ is the RT-interpolation operator ($\boldsymbol{\Pi}^{\mathbb{RT}}_h$) or the BDM-interpolation operator ($\boldsymbol{\Pi}^{\mathbb{BDM}}_h$), as appropriate.

Now, using that $(\boldsymbol{\Pi}_h\widehat{\boldsymbol{\sigma}} - \widehat{\boldsymbol{\sigma}}_h) \in \mathbb{H}^{\boldsymbol{\sigma}}_{0,h}$, the commuting diagram property (3.3) or (3.7), as appropriate, together with (2.11) and (3.17), we obtain the following

$$\mathbf{div}(\boldsymbol{\Pi}_h\widehat{\boldsymbol{\sigma}}) = \mathcal{R}_h(\mathbf{div}\,\widehat{\boldsymbol{\sigma}}) = \mathcal{R}_h(-\boldsymbol{f}) = \mathbf{div}\,\widehat{\boldsymbol{\sigma}}_h,$$

where it is straightforward that $\mathbf{div}\,(\boldsymbol{\Pi}_h\widehat{\boldsymbol{\sigma}} - \widehat{\boldsymbol{\sigma}}_h) \in \mathcal{V}_h$.

Now, using that $a_0(\cdot,\cdot)$ is coercive in $\mathcal{V}_h$, then, there exists $\overline{\alpha} > 0$ such that

$$\begin{aligned} \overline{\alpha}\|\boldsymbol{\Pi}_h\widehat{\boldsymbol{\sigma}} - \widehat{\boldsymbol{\sigma}}_h\|^2_{0,\Omega} &= \overline{\alpha}\|\boldsymbol{\Pi}_h\widehat{\boldsymbol{\sigma}} - \widehat{\boldsymbol{\sigma}}_h\|^2_{\mathbf{div},\Omega} \\ &\leq a_0(\boldsymbol{\Pi}_h\widehat{\boldsymbol{\sigma}}, \boldsymbol{\Pi}_h\widehat{\boldsymbol{\sigma}} - \widehat{\boldsymbol{\sigma}}_h) - a_0(\widehat{\boldsymbol{\sigma}}_h, \boldsymbol{\Pi}_h\widehat{\boldsymbol{\sigma}} - \widehat{\boldsymbol{\sigma}}_h) \\ &= a_0(\boldsymbol{\Pi}_h\widehat{\boldsymbol{\sigma}}, \boldsymbol{\Pi}_h\widehat{\boldsymbol{\sigma}} - \widehat{\boldsymbol{\sigma}}_h) - a_0(\widehat{\boldsymbol{\sigma}}, \boldsymbol{\Pi}_h\widehat{\boldsymbol{\sigma}} - \widehat{\boldsymbol{\sigma}}_h) - b(\boldsymbol{\Pi}_h\widehat{\boldsymbol{\sigma}} - \widehat{\boldsymbol{\sigma}}_h, \widehat{\boldsymbol{u}}) \\ &= a_0(\boldsymbol{\Pi}_h\widehat{\boldsymbol{\sigma}} - \widehat{\boldsymbol{\sigma}}, \boldsymbol{\Pi}_h\widehat{\boldsymbol{\sigma}} - \widehat{\boldsymbol{\sigma}}_h) \\ &\lesssim \|\boldsymbol{\Pi}_h\widehat{\boldsymbol{\sigma}} - \widehat{\boldsymbol{\sigma}}\|_{0,\Omega}\|\boldsymbol{\Pi}_h\widehat{\boldsymbol{\sigma}} - \widehat{\boldsymbol{\sigma}}_h\|_{0,\Omega}. \end{aligned}$$

These calculations imply that

$$\|\boldsymbol{\Pi}_h\widehat{\boldsymbol{\sigma}} - \widehat{\boldsymbol{\sigma}}_h\|_{0,\Omega} \lesssim \|\boldsymbol{\Pi}_h\widehat{\boldsymbol{\sigma}} - \widehat{\boldsymbol{\sigma}}\|_{0,\Omega}, \tag{4.4}$$

and, invoking (4.1), (4.2), (4.3) and (4.4), we have

$$\|(\boldsymbol{T} - \boldsymbol{T}_h)\boldsymbol{f}\|_{0,\Omega} \lesssim \|\widehat{\boldsymbol{u}} - \mathcal{R}_h\widehat{\boldsymbol{u}}\|_{0,\Omega} + \|\boldsymbol{\Pi}_h\widehat{\boldsymbol{\sigma}} - \widehat{\boldsymbol{\sigma}}\|_{0,\Omega}.$$

where the hidden constant is independent of h.

For the approximation error $\|(\widetilde{\boldsymbol{T}} - \widetilde{\boldsymbol{T}}_h)\boldsymbol{f}\|_{0,\Omega}$, the derivation is similar as the previous estimate. This concludes the proof. ∎

We remark that Lemma 4.1 is a general result that holds for finite elements spaces that satisfy the commuting diagram properties (3.3) or (3.7). If we are more specific in the numerical scheme, the lemma above becomes into an error estimate for each scheme.

Since we are dealing with two numerical schemes and two discrete eigenvalue problems, as corollaries, we derived the following results. The first corresponds to the approximation error between $\boldsymbol{T}$ and $\boldsymbol{T}_h$.

Corollary 4.2 (Approximation between $\boldsymbol{T}$ and $\boldsymbol{T}_h$). *Let $\boldsymbol{f} \in \mathbf{Q}^{\boldsymbol{u}}$. Under the assumptions of Theorem 2.2, if the approximation schemes $[\mathbb{P}_k]^n$-$\mathbb{RT}_k$ or $[\mathbb{P}]^n_k$-$\mathbb{BDM}_{k+1}$ are considered, then for $0 < s < k+1$, there holds*

$$\|(\boldsymbol{T} - \boldsymbol{T}_h)\boldsymbol{f}\|_{0,\Omega} \lesssim h^s\|\boldsymbol{f}\|_{0,\Omega},$$

where the hidden constant is independent of h.

Proof. If $s > 1/2$ the proof follows from (2.13), the first estimate of Lemma 4.1, the approximation properties (3.2) for RT and (3.5) for BDM, and (3.10). If $0 < s \leq 1/2$ the proof follows from (2.12), (2.13), the first estimate of Lemma 4.1, the approximation properties (3.4) for RT and (3.6) for BDM, and (3.10) ∎

Now we present the analogous of Corollary 4.2, but for the error between $\widetilde{\boldsymbol{T}}$ and $\widetilde{\boldsymbol{T}}_h$. The proof follows the same arguments of corollary above, so we skip the details.

COROLLARY 4.3 (Approximation between $\widetilde{\boldsymbol{T}}$ and $\widetilde{\boldsymbol{T}}_h$). *Let $\boldsymbol{f} \in \mathbf{Q}^{\boldsymbol{u}}$. Under the assumptions of Theorem 2.2, if the approximation schemes $[\mathbb{P}_k]^n$-$\mathbb{P}_k$-$\mathbb{RT}_k$ or $[\mathbb{P}]^n_k$-$\mathbb{P}_k$-$\mathbb{BDM}_{k+1}$ are considered, then for s as in Corollary 4.2, there holds*

$$\|(\widetilde{\boldsymbol{T}} - \widetilde{\boldsymbol{T}}_h)\boldsymbol{f}\|_{0,\Omega} \lesssim h^s \|\boldsymbol{f}\|_{0,\Omega},$$

where the hidden constant is independent of h.

As a consequence of the previous results, it is immediate that our numerical methods are spurious free, as is stated in the following result (see [19] for instance).

THEOREM 4.4. *Let $V \subset \mathbb{C}$ be an open set containing $\mathrm{sp}(\boldsymbol{T})$. Then, there exists $h_0 > 0$ such that $\mathrm{sp}(\boldsymbol{T}_h) \subset V$ for all $h < h_0$.*

4.2. Error estimates. We end the this section deriving error estimates for the eigenfunctions and eigenvalues.

Observe that according to Corollary 4.2, if $\kappa \in (0,1)$ is an isolated eigenvalue of $\boldsymbol{T}$ with multiplicity m, and $\mathcal{E}$ its associated eigenspace, then, there exist m eigenvalues $\kappa_h^{(1)}, ..., \kappa_h^{(m)}$ of $\boldsymbol{T}_h$, repeated according to their respective multiplicities, which converge to κ. Let $\mathcal{E}_h$ be the direct sum of their corresponding associated eigenspaces (see [19]). We recall the definition of the *gap* $\widehat{\delta}$ between two closed subspaces $\mathcal{X}$ and $\mathcal{Y}$ of $\mathrm{L}^2(\Omega)$:

$$\widehat{\delta}(\mathcal{X},\mathcal{Y}) := \max\left\{\delta(\mathcal{X},\mathcal{Y}), \delta(\mathcal{Y},\mathcal{X})\right\}, \text{ where } \delta(\mathcal{X},\mathcal{Y}) := \sup_{\substack{x\in\mathcal{X} \\ \|x\|_{0,\Omega}=1}} \left(\inf_{y\in\mathcal{Y}} \|x-y\|_{0,\Omega}\right).$$

The following result holds.

THEOREM 4.5. *For $k \geq 0$, the following error estimates for the eigenfunctions and eigenvalues hold*

$$\widehat{\delta}(\mathcal{E},\mathcal{E}_h) \lesssim h^{\min\{s,k+1\}} \quad \textit{and} \quad |\mu - \mu_h(i)| \lesssim h^{\min\{s,k+1\}},$$

where the hidden constants are independent of h.

Proof. The proof follows applying the results [3, 6, 7]. ∎

The next result provides a double order of convergence for the eigenvalues.

THEOREM 4.6. *For $k \geq 0$, there exists a strictly positive constant h_0 such that, for $h < h_0$ there holds*

$$|\lambda - \lambda_h| \lesssim h^{2\min\{s,k+1\}},$$

where the hidden constant is independent of h.

Proof. Let $(\lambda, \boldsymbol{\sigma}, \boldsymbol{u})$ be the solution of problem (2.10)–(2.11) and let $(\lambda_h, \boldsymbol{\sigma}_h, \boldsymbol{u}_h)$ be the solution of problem (3.13)–(3.14) with $\|\boldsymbol{u}_h\|_{0,\Omega} = \|\boldsymbol{u}\|_{0,\Omega} = 1$. The following identity can be followed from the proof of Lemma 4 of [12]

$$\lambda - \lambda_h = \frac{1}{2\mu}\|\boldsymbol{\sigma}^d - \boldsymbol{\sigma}_h^d\|_{0,\Omega}^2 - \lambda_h\|\boldsymbol{u} - \boldsymbol{u}_h\|_{0,\Omega}^2.$$

Then

$$|\lambda - \lambda_h| \lesssim \|\boldsymbol{\sigma} - \boldsymbol{\sigma}_h\|_{0,\Omega}^2 + \|\boldsymbol{u} - \boldsymbol{u}_h\|_{0,\Omega}^2,$$

where the hidden constant is independent of h. The proof is completed with an application of the estimate given in [31, Theorem 11.2], together with properties (3.8)–(3.10), the additional regularity result given in Theorem 2.2 and the first equation of (2.1). ∎

5. Numerical experiments. In this section we report some numerical tests in order to assess the performance of the proposed mixed element method, in the computation of the eigenvalues of problem (3.11)–(3.12). In all our experiments we consider the boundary condition $\boldsymbol{u} = 0$ and $\mu = 1/2$.

We have implemented the discrete eigenvalue problem in a FEniCS code [24, 1]. The rates of convergence have been computed with a least-square fitting.

The schemes are tested in two-dimensional and three-dimensional domains under different geometrical conditions, such as convexity, non-convexity or curved domains. For all the geometric configurations, we compute the lowest eigenvalues and convergence orders. For the two-dimensional domains we prove the schemes with polynomials degrees $k = 0, 1, 2$, except in the 3-D domains, where we only consider $k = 0$ due to limitations of machine memory. With the computed results at hand, we compare the schemes that only differ on the $\mathbb{H}(\mathrm{div})$ finite element space. Let us remark that, for the first test, we have also programmed the reduced scheme (3.13)–(3.14), but there is no significant change in the approximation results. This allows us to perform the rest of the numerical tests with the scheme (3.11)–(3.12), which provides the pressure in the preprocess. However, for computational efficiency purposes, the choice of (3.13)–(3.14) is preferred because it is simpler and involves fewer degrees of freedom. This becomes an important factor in three-dimensional problems (see Section 5.4 below).

In what follows, N denotes the mesh resolution, with $h \sim N^{-1}$, and dof denotes the degrees of freedom, which will depends on the numerical scheme used.

In each test we also report plots of the associated eigenfunctions, in particular the velocity fields and pressure fluctuations. Moreover, in several experiments we consider the relative errors e_{λ_i} $i = 1, 2, 3, 4$ for different choices of k, where

$$e_{\lambda_i} := \frac{|\lambda_{h_i} - \lambda_{extr_i}|}{|\lambda_{extr_i}|}.$$

Finally, we denote by $e_{\lambda_i}(\mathbb{RT})$ and $e_{\lambda_i}(\mathbb{BDM})$ the relative errors obtained using $[\mathbb{P}_k]^n$-$\mathbb{P}_k$-$\mathbb{RT}_k$ and $[\mathbb{P}_k]^n$-$\mathbb{P}_k$-$\mathbb{BDM}_{k+1}$ schemes, respectively.

5.1. Test 1: Square. In this test we consider as computational domain the square $\Omega := (-1, 1)^2$, where the number of elements scales as $2N^2$. The meshes for the following tests are the presented in Figure 1. We observe that the convexity of this domain leads to sufficiently smooth eigenfunctions for the Stokes eigenvalue problem. This fact implies that the order of convergence will be optimal. The polynomial degrees considered for the test are $k = 0, 1, 2$.

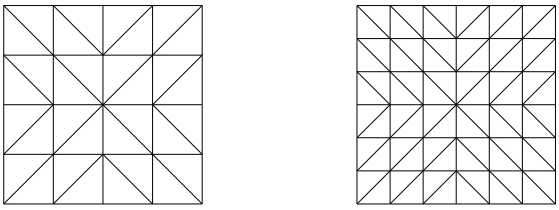

FIG. 1. *Test 1. Examples of the meshes used in the unit square. The left figure represents a mesh for $N = 4$ and the right one for $N = 6$.*

TABLE 1

Test 1. Lowest computed eigenvalues for polynomial degrees $k = 0, 1, 2$ using the $[\mathbb{P}_k]^n$-$\mathbb{P}_k$-$\mathbb{RT}_k$ scheme.

k	$N = 10$	$N = 20$	$N = 30$	$N = 40$	Order	λ_{extr}	[26]	[25]
0	13.18205	13.10744	13.09534	13.09127	2.21	13.08688	13.0860	13.086
	21.08840	22.63791	22.85202	22.93446	2.40	22.99702	23.0308	23.031
	21.33183	22.69036	22.88083	22.93810	2.46	22.99245	23.0308	23.031
	27.96811	31.27226	31.70100	31.81983	2.59	31.93357	32.0443	32.053
	33.42538	37.66786	38.18478	38.32443	2.69	38.44565	38.5252	38.532
1	13.08698	13.08620	13.08617	13.08617	4.56	13.08617	13.0860	13.086
	23.04310	23.03182	23.03123	23.03114	4.04	23.03109	23.0308	23.031
	23.04310	23.03182	23.03123	23.03114	4.04	23.03109	23.0308	23.031
	32.07944	32.05400	32.05270	32.05249	4.07	32.05239	32.0443	32.053
	38.60095	38.53594	38.53227	38.53165	3.92	38.53134	38.5252	38.532
2	13.08528	13.08616	13.08617	13.08617	5.84	13.08617	13.0860	13.086
	23.03116	23.03109	23.03109	23.03109	6.00	23.03109	23.0308	23.031
	23.03116	23.03109	23.03109	23.03109	6.00	23.03109	23.0308	23.031
	32.05268	32.05239	32.05239	32.05239	6.00	32.05239	32.0443	32.053
	38.53256	38.53138	38.53136	38.53136	5.97	38.53136	38.5252	38.532

TABLE 2

Test 1. Lowest computed eigenvalues for polynomial degrees $k = 0, 1, 2$ using the $[\mathbb{P}_k]^n$-$\mathbb{P}_k$-$\mathbb{BDM}_{k+1}$ scheme.

k	$N = 10$	$N = 20$	$N = 30$	$N = 40$	Order	λ_{extr}	[26]	[25]
0	13.39520	13.16477	13.12123	13.10591	1.97	13.08574	13.0860	13.086
	23.74378	23.22000	23.11593	23.07899	1.89	23.02641	23.0308	23.031
	24.19514	23.32856	23.16384	23.10587	1.96	23.02865	23.0308	23.031
	33.73344	32.50272	32.25523	32.16703	1.87	32.03920	32.0443	32.053
	41.15209	39.23059	38.84532	38.70858	1.88	38.51262	38.5252	38.532
1	13.08919	13.08636	13.08621	13.08618	3.99	13.08617	13.0860	13.086
	23.04441	23.03195	23.03126	23.03115	3.96	23.03109	23.0308	23.031
	23.05331	23.03253	23.03138	23.03118	3.95	23.03109	23.0308	23.031
	32.10055	32.0555	32.05302	32.05259	3.92	32.05238	32.0443	32.053
	38.61259	38.53671	38.53243	38.53170	3.92	38.53134	38.5252	38.532
2	13.08618	13.08617	13.08617	13.08617	6.16	13.08617	13.0860	13.086
	23.03117	23.03109	23.03109	23.03109	6.04	23.03109	23.0308	23.031
	23.03128	23.03110	23.03109	23.03109	6.01	23.03109	23.0308	23.031
	32.05303	32.05240	32.05239	32.05239	6.02	32.05239	32.0443	32.053
	38.53239	38.53138	38.53136	38.53136	5.92	38.53136	38.5252	38.532

In Table 1 we report the first five eigenvalues computed with the $[\mathbb{P}_k]^n$-$\mathbb{P}_k$-$\mathbb{RT}_k$ scheme, considering different meshes and polynomial degrees. In the column λ_{extr} we report extrapolated values, obtained with a least square fitting, which we compare with two well known references that have dealt with the same domain. We observe that

our extrapolated values are close to those in [26, 25] and that the rates of convergence are as we expect. In fact, we notice that for $k = 0$, the order of approximation is clearly $\mathcal{O}(h^2)$, meanwhile for $k > 0$ the observed order is close to $\mathcal{O}(h^{2(k+1)}) \simeq \mathcal{O}(\text{dof}^{-(k+1)})$.

On the other hand, Table 2 shows the computed eigenvalues when using the $[\mathbb{P}_k]^n$-$\mathbb{P}_k$-$\mathbb{BDM}_{k+1}$ scheme, where we observe that an optimal rate of convergence $\mathcal{O}(h^{2(k+1)})$ is reached for high order elements. For instance, in Figure 3 we observe that, except for the noise present in the error slopes, the scheme allows to stay on the optimal rate of convergence. To complete the experiment, we present in Figure 2 the first, third and fourth lowest computed eigenfunctions on the square domain, and in Figure 3 we present the error behavior on the chosen numerical schemes.

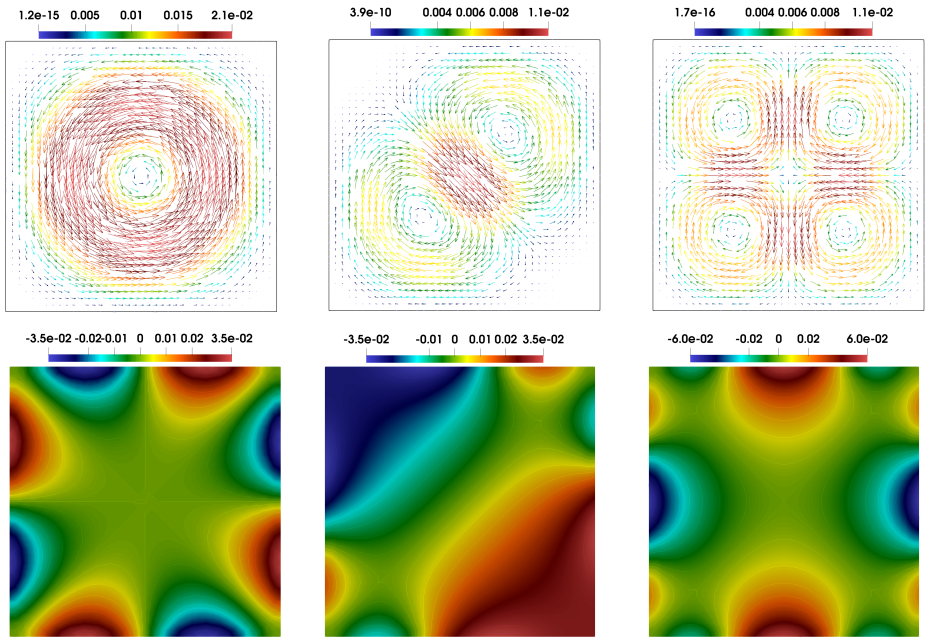

FIG. 2. *Test 1. Approximate velocity field $\boldsymbol{u}_h$ (top row) and pressure p_h (bottom row), corresponding to the first, third and fourth lowest eigenvalues in the square domain.*

5.2. Test 2: Circular domain. In this test we consider the unit circle as computational domain, which we define by $\Omega := \{(x, y) \in \mathbb{R}^2 \, : \, x^2 + y^2 \leq 1\}$. The relevance of this experiment is that we are approximating a curved domain with triangular meshes, which lead to a variational crime. In Figure 4 we present examples of the quasi-uniform triangular meshes considered to approximate the circular domain.

The fact that we are approximating a curved domain by means of a polygonal one is reflected in the numerical experiments presented below in Table 3 where, independent of the polynomial degree, the order of convergence is $\mathcal{O}(h^2) \simeq \mathcal{O}(\text{dof}^{-1})$ for all $k \geq 0$. The results from using the $[\mathbb{P}_k]^n$-$\mathbb{P}_k$-$\mathbb{BDM}_{k+1}$ scheme are described in Table 4, where similar rates of convergence are observed. We recall that N represents the mesh resolution such that the number of elements is $6N^2$. In Figure 5 we present the approximated eigenfunctions for the lowest frequencies. We further describe the results obtained in Figure 6, where we observe the experimental rates obtained, which are in good agreement with those predicted by theory.

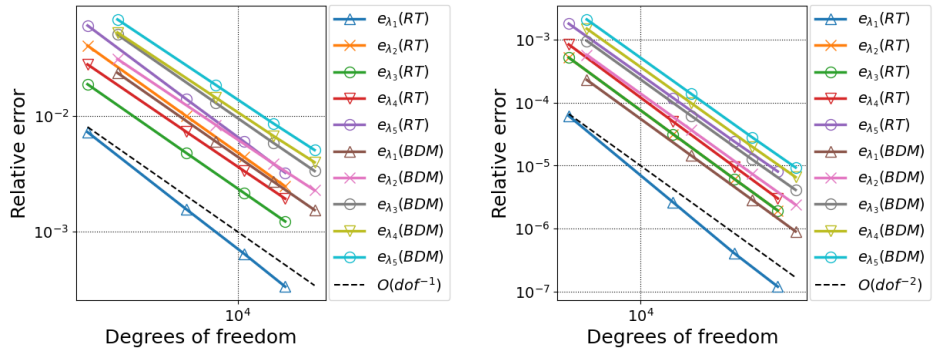

FIG. 3. *Test 1. Comparison of the eigenvalues error behavior in the square domain using the* $[\mathbb{P}_k]^n$-$\mathbb{P}_k$-$\mathbb{RT}_k$ *and* $[\mathbb{P}_k]^n$-$\mathbb{P}_k$-$\mathbb{BDM}_{k+1}$ *schemes. The experiment considers polynomials of degree* $k = 0$ *(left) and* $k = 1$ *(right).*

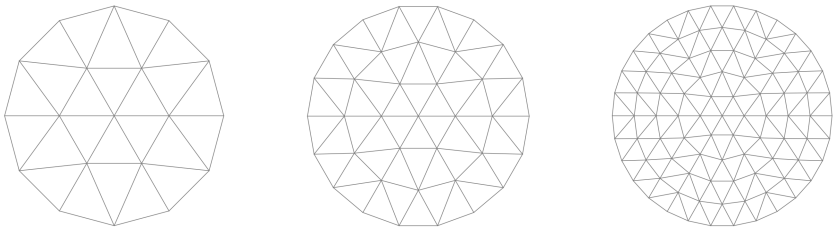

FIG. 4. *Test 2. Meshes used in the circular domain.*

TABLE 3
Test 2. Lowest computed eigenvalues for polynomial degrees $k = 0, 1, 2$ *using the* $[\mathbb{P}_k]^n$-$\mathbb{P}_k$-$\mathbb{RT}_k$ *scheme.*

k	$N = 20$	$N = 30$	$N = 40$	$N = 50$	Order	λ_{extr}	[21]
0	14.94827	14.79867	14.74712	14.72354	2.04	14.68251	14.68345
	26.81747	26.56803	26.48211	26.44329	2.05	26.37559	26.37840
	26.81821	26.56845	26.48262	26.44365	2.06	26.37683	26.37862
	41.32838	40.98177	40.85915	40.80453	2.01	40.70533	40.71434
	41.34096	40.98359	40.86093	40.80487	2.05	40.70809	40.71606
1	14.94196	14.79448	14.74448	14.72169	2.08	14.68323	14.68345
	26.84091	26.57657	26.48686	26.44594	2.08	26.37704	26.37840
	26.84099	26.57662	26.48687	26.44595	2.08	26.37703	26.37862
	41.42501	41.01797	40.87964	40.81652	2.08	40.71046	40.71434
	41.42543	41.01805	40.87966	40.81654	2.08	40.71037	40.71606
2	14.94315	14.79487	14.74464	14.72177	2.09	14.68361	14.68345
	26.84301	26.57727	26.48715	26.44610	2.08	26.37680	26.37840
	26.84303	26.57728	26.48716	26.44610	2.08	26.37680	26.37862
	41.42807	41.01900	40.88008	40.81675	2.08	40.71012	40.71434
	41.42814	41.01902	40.88008	40.81676	2.08	40.71010	40.71606

5.3. Test 3: The L-Shape domain.. In this numerical test we consider an L-shape domain given by $\Omega := (-1,1) \times (-1,1) \backslash \big((-1,0) \times (-1,0)\big)$. In Table 5 we report the results when using $[\mathbb{P}_k]^n$-$\mathbb{P}_k$-$\mathbb{RT}_k$ and $[\mathbb{P}_k]^n$-$\mathbb{P}_k$-$\mathbb{BDM}_{k+1}$ schemes to solve the discrete eigenvalue problem. Note that the singularity produced by the reentrant corner yields to a rate of convergence around 1.7 (see [25] for instance), as can be seen in the lowest computed eigenvalue. In fact, we observe that the order of convergence

TABLE 4

Test 2. Lowest computed eigenvalues for polynomial degrees $k=0,1,2$ using the $[\mathbb{P}_k]^n$-$\mathbb{P}_k$-$\mathbb{BDM}_{k+1}$ scheme.

k	$N=20$	$N=30$	$N=40$	$N=50$	Order	λ_{extr}	[21]
0	14.82469	14.71768	14.69784	14.69090	2.00	14.68199	14.68345
	26.77392	26.47427	26.41889	26.39951	2.00	26.37450	26.37840
	26.77392	26.47427	26.41889	26.39951	2.00	26.37450	26.37862
	41.56881	40.92423	40.80343	40.76105	1.98	40.70545	40.71434
	41.56881	40.92423	40.80343	40.76105	1.98	40.70545	40.71606
1	14.70933	14.68872	14.68496	14.68365	2.02	14.68199	14.68345
	26.42481	26.38682	26.38000	26.37764	2.05	26.37473	26.37840
	26.42481	26.38682	26.38000	26.37764	2.05	26.37703	26.37862
	40.78741	40.72552	40.71483	40.71115	2.11	40.70686	40.71434
	40.78741	40.72552	40.71483	40.71115	2.11	40.70686	40.71606
2	14.70930	14.68873	14.68496	14.68365	2.02	14.68200	14.68345
	26.42370	26.38677	26.38000	26.37764	2.02	26.37467	26.37840
	26.42370	26.38677	26.38000	26.37764	2.02	26.37467	26.37862
	40.78222	40.72523	40.71478	40.71113	2.02	40.70655	40.71434
	40.78222	40.72523	40.71478	40.71113	2.02	40.70655	40.71606

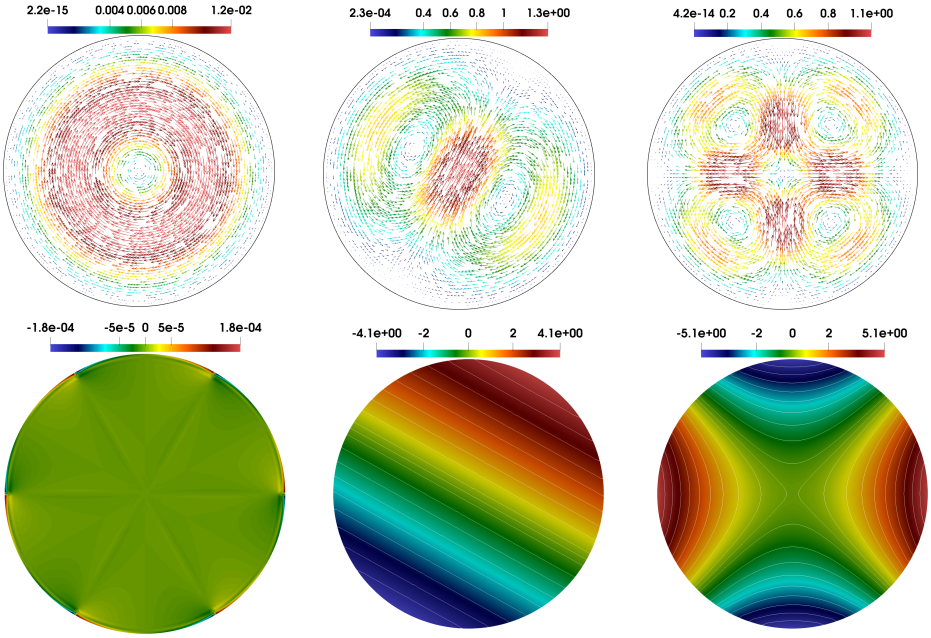

FIG. 5. *Test 2. Approximate velocity field $\boldsymbol{u}_h$ (top row) and pressure p_h (bottom row), corresponding to the first, third and fourth lowest eigenvalues in the unit circular domain.*

is $2s \geq 1.08$, as is predictable in this geometry. For better visualization, we explore this result in the relative error plots in Figure 7, where the slopes are compared with $\mathcal{O}(\text{dof}^{-\sqrt{3}/2}) \simeq \mathcal{O}(h^{1.7})$, which is the best order possible with uniform refinements.

We end this test reporting plots of the velocity fields and pressure fluctuations in Figure 8 where, as is expectable, high gradients around the singularity are observed.

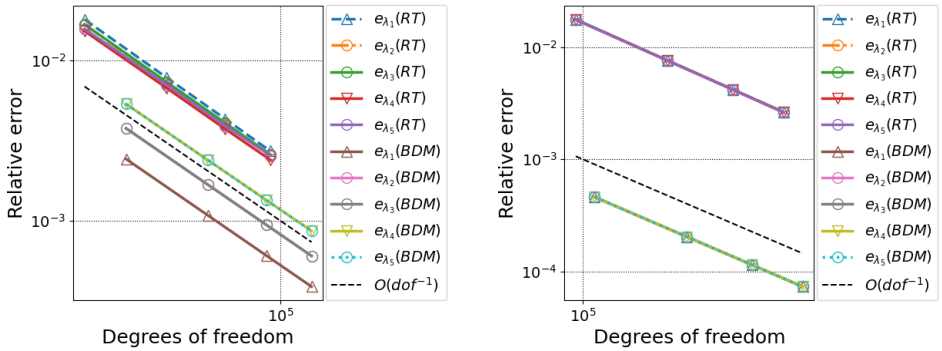

FIG. 6. *Test 2. Comparison of the eigenvalues error behavior in the circle using the* $[\mathbb{P}_k]^n$-$\mathbb{P}_k$-$\mathbb{RT}_k$ *and* $[\mathbb{P}_k]^n$-$\mathbb{P}_k$-$\mathbb{BDM}_{k+1}$ *schemes. The experiment considers polynomials of degree* $k = 0$ *(left) and* $k = 2$ *(right).*

TABLE 5
Test 3. Lowest computed eigenvalues for polynomial degrees $k = 0$ *in the L-shape domain.*

Scheme	$N = 9$	$N = 15$	$N = 20$	$N = 35$	Order	λ_{extr}
$[\mathbb{P}_k]^n$-$\mathbb{P}_k$-$\mathbb{RT}_k$	29.43565	30.83700	31.16193	31.62598	1.59	31.89457
	34.98077	36.28132	36.50660	36.83669	2.03	36.94231
	40.70064	41.43833	41.62290	41.83014	1.73	41.94524
	46.83830	48.22776	48.47328	48.80875	2.07	48.91635
	52.08483	53.96541	54.48404	55.02474	1.65	55.37238
$[\mathbb{P}_k]^n$-$\mathbb{P}_k$-$\mathbb{BDM}_{k+1}$	32.59542	32.24970	32.14635	32.06144	1.75	32.00483
	38.76953	37.57884	37.32081	37.11240	2.26	37.03276
	44.76985	42.88018	42.46067	42.10765	2.19	41.96744
	52.09587	50.19205	49.67367	49.20827	1.81	48.93475
	58.84979	56.72442	56.20364	55.63553	1.79	55.33628

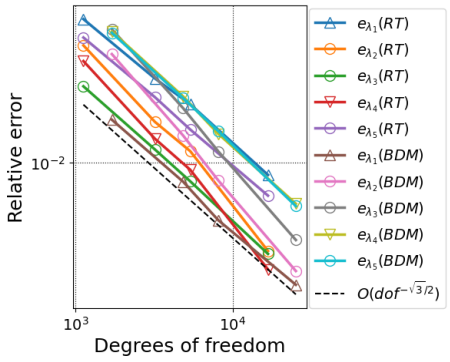

FIG. 7. *Test 3. Comparison of the eigenvalues error behavior in the L-shape domain using the* $[\mathbb{P}_k]^n$-$\mathbb{P}_k$-$\mathbb{RT}_k$ *and* $[\mathbb{P}_k]^n$-$\mathbb{P}_k$-$\mathbb{BDM}_{k+1}$ *schemes. The experiment considers polynomials of degree* $k = 0$.

5.4. 3-D test. This test aims to confirm the accuracy of the proposed schemes on three dimensions. To this end, we consider two scenarios: the first one considers a cube in the region $\Omega = (0, 1)^3$, which we will use as a benchmark. Here, N scales as the number of cells such that the number of tetrahedrons is $6(N+1)^3$ and $N \sim \text{dof}^{1/3}$.

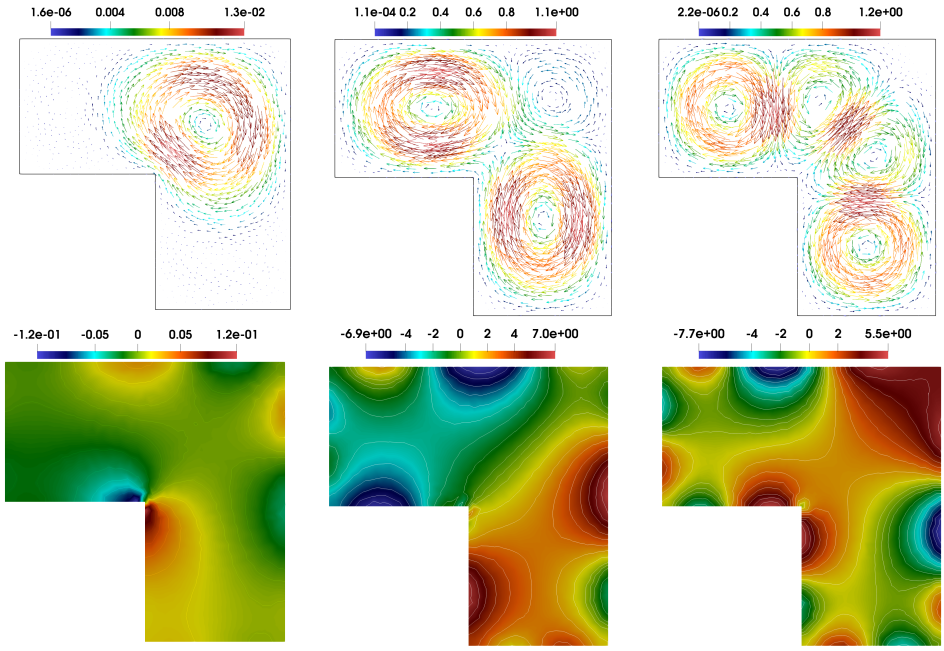

FIG. 8. *Test 3. Approximate velocity field $\boldsymbol{u}_h$ (top row) and pressure p_h (bottom row), corresponding to the first, third and fourth lowest eigenvalues in the L-shape domain.*

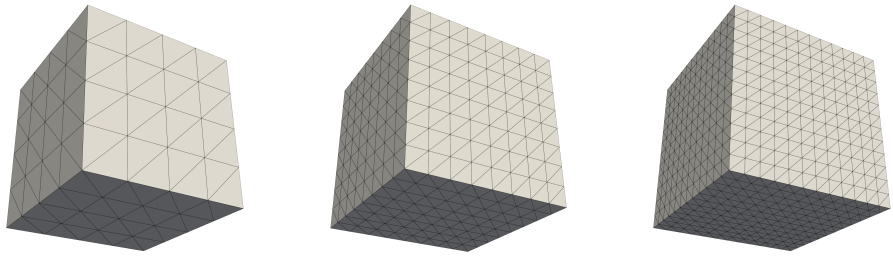

FIG. 9. *3-D test. Examples of the meshes used in the unit cube. Left: mesh with $N = 4$. Middle: mesh with $N = 8$. Right: mesh with $N = 12$.*

In Figure 9 we present examples of the meshes used in the cube domain. In the second scenario we consider the unit sphere $\Omega := \{(x, y, z) \in \mathbb{R}^3 : x^2 + y^2 + z^2 \leq 1\}$. For this case, the mesh resolution is such that $N \sim \text{dof}^{1/3}$. We remark that this test consists into approximate a curved domain by means of tetrahedral meshes. In Figure 10 we present examples of the meshes used in the experiment

The convergence results from using the lowest order approximations $[\mathbb{P}_0]^n$-$\mathbb{P}_0$-$\mathbb{RT}_0$ and $[\mathbb{P}_0]^n$-$\mathbb{P}_0$-$\mathbb{BDM}_1$ schemes in the unit cube domain are reported in Table 6. In Figure 13 we present the relative error plot for the approximated eigenvalues compared with the extrapolated ones on each table. Clearly the expected rate of convergence $\mathcal{O}(h^2) \simeq O(\text{dof}^{-2/3})$ is attained. Together with this, the second and fourth lowest eigenfunctions corresponding to $\boldsymbol{u}_h$ and p_h are depicted in Figure 12. We complete the benchmarking with a computational cost test. Classical approaches such as Taylor-Hood elements $(\mathbb{P}_2 - \mathbb{P}_1)$, $\mathbb{P}_2 - \mathbb{P}_0$ and mini-element $(\mathbb{P}_{1+b} - \mathbb{P}_1)$, where the subscript

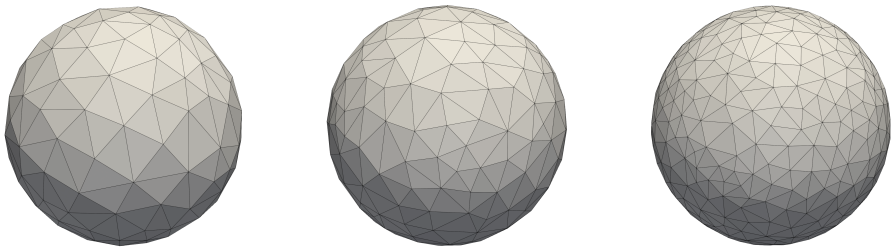

FIG. 10. *3-D test. Examples of the meshes used in the unit sphere. The left figure represents a mesh for $N = 8$, the middle figure for $N = 10$ and the right figure for $N = 14$.*

b denotes the corresponding bubble functions, are considered. The test is performed by measuring memory consumption (MiB), flops counting double precision operations (DPOPS), and execution times when solving the eigenvalue problem (preprocessing), and extracting the first eigenfunction with the corresponding computation of additional variables (postprocessing). The results obtained are reported in Figure 11, where we observe that the $[\mathbb{P}_0]^3$-$\mathbb{P}_0$-$\mathbb{BDM}_1$, together with its reduced version are the most expensive schemes, and hence slower, than the others. On the other hand, it is observed that the $[\mathbb{P}_0]^3$-$\mathbb{P}_0$-$\mathbb{RT}_0$ and $[\mathbb{P}_0]^3$-$\mathbb{RT}_0$ schemes executes less DPOPS and consumes less memory than Taylor-Hood and $\mathbb{P}_2$-$\mathbb{P}_0$ schemes. For instance, we observe that they are almost at par with the performance of the mini-element, which is a scheme well known for its efficiency and low cost. Also, comparing the performance of the complete and reduced schemes shows that setting the pressure as a variable in the system is virtually free of charge.

We finish this section by presenting the results on the unit sphere case. The convergence results are presented in Table 7. It notes that the proposed methods work perfectly and deliver the expected double order of convergence $\mathcal{O}(h^2) \simeq O(\text{dof}^{-2/3})$ for both schemes, which is observed in Figure 13. For completeness, in Figure 14 we present plots of the approximated velocity fields and pressure fluctuations associated with the second and fourth lowest eigenvalues.

TABLE 6
3-D test. Lowest computed eigenvalues for polynomial degrees $k = 0$ in the unit cube domain.

Scheme	$N = 12$	$N = 14$	$N = 20$	$N = 22$	Order	λ_{extr}
$[\mathbb{P}_k]^n$-$\mathbb{P}_k$-$\mathbb{RT}_k$	61.80994	61.90155	62.03636	62.05956	1.85	62.18158
	61.88835	61.95891	62.06425	62.08258	1.80	62.18191
	61.88835	61.95891	62.06425	62.08258	1.80	62.18191
	91.46148	91.50688	91.56815	91.57848	2.17	91.62161
	91.46148	91.50688	91.56815	91.57848	2.17	91.62161
$[\mathbb{P}_k]^n$-$\mathbb{P}_k$-$\mathbb{BDM}_{k+1}$	63.01698	62.79574	62.48018	62.42719	1.99	62.17158
	63.19549	62.92786	62.54560	62.48136	1.98	62.16910
	63.19549	62.92786	62.54560	62.48136	1.98	62.16910
	93.80876	93.24861	92.43604	92.29798	1.92	91.60166
	93.80876	93.24861	92.43604	92.29798	1.92	91.60166

6. Conclusions. From our analysis and numerical tests, we derive the following conclusions:

- The proposed numerical schemes in our study perform an accurate approximation of the eigenvalues and the associated eigenfunctions in two and three

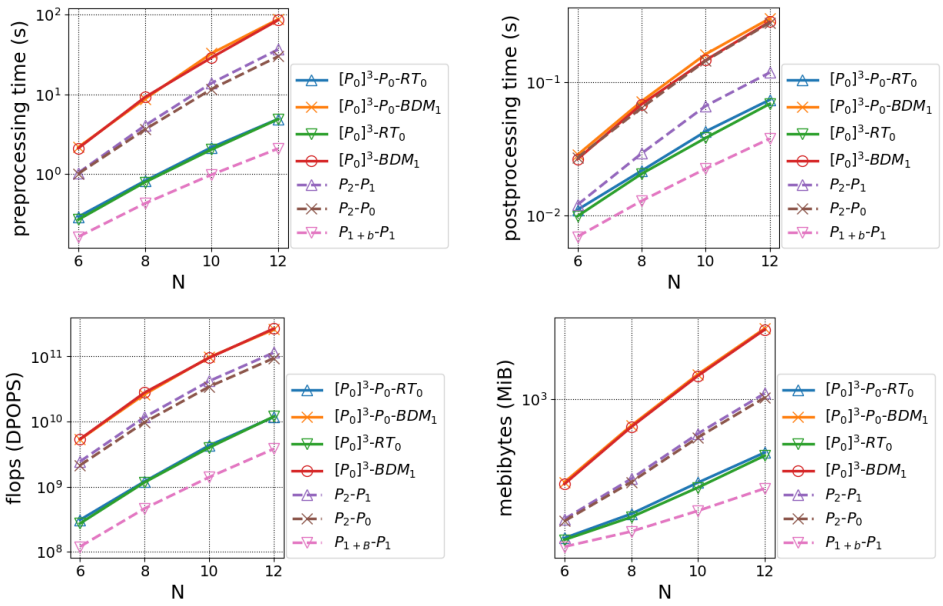

FIG. 11. *3-D test. Comparison of computational cost in the eigenvalue problem on the 3D unit cube. The test considers the lowest order approximation on the augmented schemes ($k = 0$).*

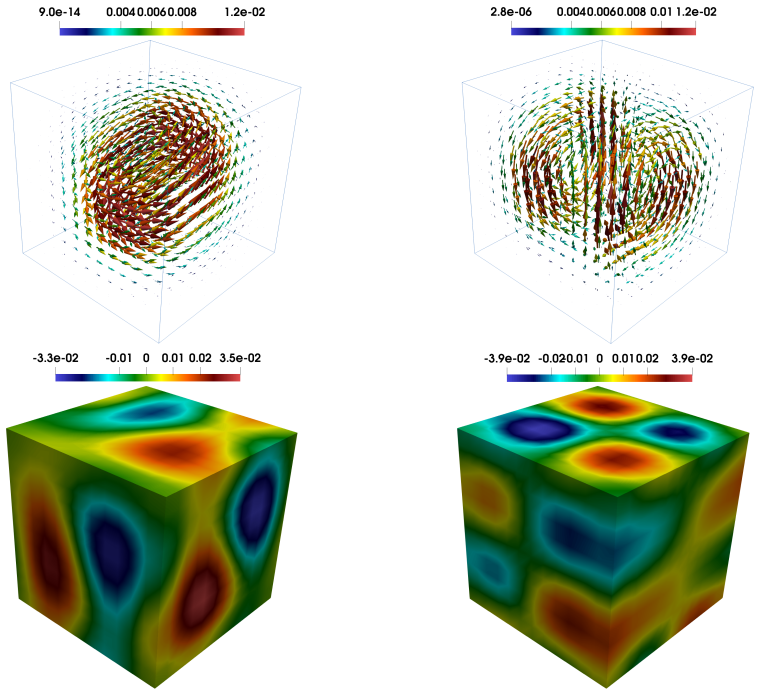

FIG. 12. *3-D test. Approximated velocity field $\boldsymbol{u}_h$ (top) and pressure p (bottom), corresponding to the second and fourth lowest eigenvalues in the unit cube domain.*

TABLE 7
3-D test. Lowest computed eigenvalues for polynomial degrees $k = 0$ in the unit sphere domain.

Scheme	$N = 15$	$N = 20$	$N = 25$	$N = 30$	Order	λ_{extr}
$[\mathbb{P}_k]^n$-$\mathbb{P}_k$-$\mathbb{RT}_k$	20.62250	20.52408	20.47658	20.45165	1.91	20.38910
	20.62132	20.52159	20.47604	20.45127	2.02	20.39546
	20.61793	20.52068	20.47512	20.45118	1.99	20.39463
	33.42601	33.50029	33.52026	33.53321	3.40	33.54308
	33.43630	33.50574	33.52060	33.53473	3.57	33.54138
$[\mathbb{P}_k]^n$-$\mathbb{P}_k$-$\mathbb{BDM}_{k+1}$	20.92522	20.68859	20.58360	20.52646	2.10	20.40504
	20.92301	20.68732	20.58268	20.52622	2.10	20.40513
	20.92037	20.68576	20.58228	20.52572	2.11	20.40671
	34.64358	34.18189	33.94945	33.83133	1.82	33.50504
	34.65002	34.18387	33.95073	33.83166	1.83	33.50625

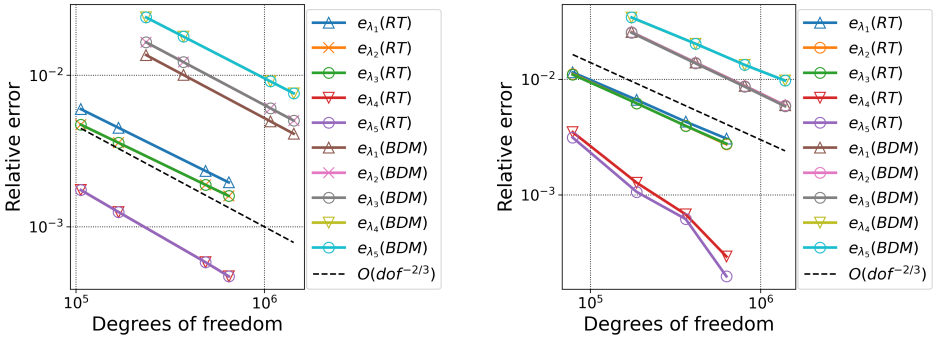

FIG. 13. *3-D test. Comparison of the relative error behavior in the unit cube (left) and the unit sphere (right) when using $[\mathbb{P}_k]^n$-$\mathbb{P}_k$-$\mathbb{RT}_k$ and $[\mathbb{P}_k]^n$-$\mathbb{P}_k$-$\mathbb{BDM}_{k+1}$ schemes.*

dimensions.

- For curved domains both schemes work perfectly in two and three dimensions.
- For the lowest order in both numerical schemes ($k = 0$) the double order of convergence is clearly quadratic and, for $k \geq 1$, the $[\mathbb{P}_k]^n$-$\mathbb{P}_k$-$\mathbb{BDM}_{k+1}$ scheme seems to be more stable than the $[\mathbb{P}_k]^n$-$\mathbb{P}_k$-$\mathbb{RT}_k$ when the orders of convergence are computed. This is due to the fact that, when $[\mathbb{P}_k]^n$-$\mathbb{P}_k$-$\mathbb{RT}_k$ is considered, the computed eigenvalues are more close between them than the scheme with BDM elements. This phenomenon is observable in the relative error plots. However, it is preferable to choose the schemes with Raviart-Thomas elements due to the efficiency and accuracy of the approximation.
- In non convex domains, the results are the expectable due to the singularity of the geometry. This is an interesting fact that motivates the analysis of adaptive schemes.

REFERENCES

[1] M. S. ALNÆS, J. BLECHTA, J. HAKE, A. JOHANSSON, B. KEHLET, A. LOGG, C. RICHARDSON, J. RING, M. E. ROGNES, AND G. N. WELLS, *The fenics project version 1.5*, Archive of Numerical Software, 3 (2015), https://doi.org/10.11588/ans.2015.100.20553.

[2] P. F. ANTONIETTI, A. BUFFA, AND I. PERUGIA, *Discontinuous Galerkin approximation of the Laplace eigenproblem*, Comput. Methods Appl. Mech. Engrg., 195 (2006), pp. 3483–3503, https://doi.org/10.1016/j.cma.2005.06.023.

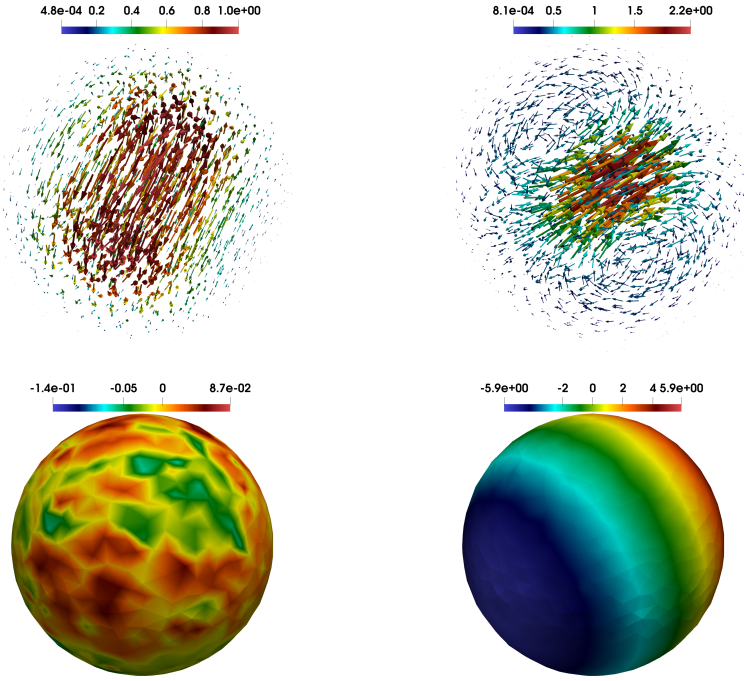

FIG. 14. *Approximated velocity field* $\boldsymbol{u}_h$ *(top) and pressure* p_h *(bottom), corresponding to the second and fourth lowest eigenvalues in the unit sphere domain.*

[3] I. Babuška and J. Osborn, *Handbook of numerical analysis. Vol. II*, (1991), pp. x+928. Finite element methods. Part 1.

[4] D. Boffi, *Finite element approximation of eigenvalue problems*, Acta Numer., 19 (2010), pp. 1–120, https://doi.org/10.1017/S0962492910000012.

[5] D. Boffi, F. Brezzi, and M. Fortin, *Mixed finite element methods and applications*, vol. 44 of Springer Series in Computational Mathematics, Springer, Heidelberg, 2013, https://doi.org/10.1007/978-3-642-36519-5.

[6] D. Boffi, F. Brezzi, and L. Gastaldi, *On the convergence of eigenvalues for mixed formulations*, vol. 25, 1997, pp. 131–154 (1998), http://www.numdam.org/item?id=ASNSP_1997_4_25_1-2_131_0. Dedicated to Ennio De Giorgi.

[7] D. Boffi, F. Brezzi, and L. Gastaldi, *On the problem of spurious eigenvalues in the approximation of linear elliptic problems in mixed form*, Math. Comp., 69 (2000), pp. 121–140, https://doi.org/10.1090/S0025-5718-99-01072-8, https://doi-org.usm.idm.oclc.org/10.1090/S0025-5718-99-01072-8.

[8] F. Brezzi, J. Douglas, Jr., and L. D. Marini, *Two families of mixed finite elements for second order elliptic problems*, Numer. Math., 47 (1985), pp. 217–235, https://doi.org/10.1007/BF01389710.

[9] F. Brezzi and M. Fortin, *Mixed and hybrid finite element methods*, vol. 15 of Springer Series in Computational Mathematics, Springer-Verlag, New York, 1991, https://doi.org/10.1007/978-1-4612-3172-1.

[10] A. Buffa, P. Houston, and I. Perugia, *Discontinuous Galerkin computation of the Maxwell eigenvalues on simplicial meshes*, J. Comput. Appl. Math., 204 (2007), pp. 317–333, https://doi.org/10.1016/j.cam.2006.01.042.

[11] Z. Cai, C. Tong, P. S. Vassilevski, and C. Wang, *Mixed finite element methods for incompressible flow: stationary Stokes equations*, Numer. Methods Partial Differential Equations, 26 (2010), pp. 957–978, https://doi.org/10.1002/num.20467.

[12] R. G. Durán, L. Gastaldi, and C. Padra, *A posteriori error estimators for mixed approximations of eigenvalue problems*, Math. Models Methods Appl. Sci., 9 (1999), pp. 1165–1178, https://doi.org/10.1142/S021820259900052X.

[13] E. B. Fabes, C. E. Kenig, and G. C. Verchota, *The Dirichlet problem for the Stokes system*

on Lipschitz domains, Duke Math. J., 57 (1988), pp. 769–793, https://doi.org/10.1215/S0012-7094-88-05734-1.

[14] F. Gardini, *Mixed approximation of eigenvalue problems: a superconvergence result*, M2AN Math. Model. Numer. Anal., 43 (2009), pp. 853–865, https://doi.org/10.1051/m2an/2009005.

[15] G. N. Gatica, A. Márquez, and M. A. Sánchez, *Analysis of a velocity-pressure-pseudostress formulation for the stationary Stokes equations*, Comput. Methods Appl. Mech. Engrg., 199 (2010), pp. 1064–1079, https://doi.org/10.1016/j.cma.2009.11.024.

[16] J. Gedicke and A. Khan, *Arnold-Winther mixed finite elements for Stokes eigenvalue problems*, SIAM J. Sci. Comput., 40 (2018), pp. A3449–A3469, https://doi.org/10.1137/17M1162032.

[17] J. Gedicke and A. Khan, *Divergence-conforming discontinuous Galerkin finite elements for Stokes eigenvalue problems*, Numer. Math., 144 (2020), pp. 585–614, https://doi.org/10.1007/s00211-019-01095-x.

[18] R. Hiptmair, *Finite elements in computational electromagnetism*, Acta Numer., 11 (2002), pp. 237–339, https://doi.org/10.1017/S0962492902000041.

[19] T. Kato, *Perturbation theory for linear operators*, Die Grundlehren der mathematischen Wissenschaften, Band 132, Springer-Verlag New York, Inc., New York, 1966.

[20] F. Lepe, S. Meddahi, D. Mora, and R. Rodríguez, *Mixed discontinuous Galerkin approximation of the elasticity eigenproblem*, Numer. Math., 142 (2019), pp. 749–786, https://doi.org/10.1007/s00211-019-01035-9.

[21] F. Lepe and D. Mora, *Symmetric and nonsymmetric discontinuous Galerkin methods for a pseudostress formulation of the Stokes spectral problem*, SIAM J. Sci. Comput., 42 (2020), pp. A698–A722, https://doi.org/10.1137/19M1259535.

[22] F. Lepe, D. Mora, and R. Rodríguez, *Finite element analysis of a bending moment formulation for the vibration problem of a non-homogeneous Timoshenko beam*, J. Sci. Comput., 66 (2016), pp. 825–848, https://doi.org/10.1007/s10915-015-0046-z.

[23] F. Lepe and G. Rivera, *A virtual element approximation for the pseudostress formulation of the Stokes eigenvalue problem*, Comput. Methods Appl. Mech. Engrg., 379 (2021), pp. Paper No. 113753, 21, https://doi.org/10.1016/j.cma.2021.113753, https://doi.org/10.1016/j.cma.2021.113753.

[24] A. Logg, K.-A. Mardal, and G. Wells, *Automated solution of differential equations by the finite element method: The FEniCS book*, vol. 84, Springer Science & Business Media, 2012, https://doi.org/https://doi.org/10.1007/978-3-642-23099-8.

[25] C. Lovadina, M. Lyly, and R. Stenberg, *A posteriori estimates for the Stokes eigenvalue problem*, Numer. Methods Partial Differential Equations, 25 (2009), pp. 244–257, https://doi.org/10.1002/num.20342.

[26] S. Meddahi, D. Mora, and R. Rodríguez, *A finite element analysis of a pseudostress formulation for the Stokes eigenvalue problem*, IMA J. Numer. Anal., 35 (2015), pp. 749–766, https://doi.org/10.1093/imanum/dru006.

[27] J. Meng, Y. Zhang, and L. Mei, *A virtual element method for the Laplacian eigenvalue problem in mixed form*, Appl. Numer. Math., 156 (2020), pp. 1–13, https://doi.org/10.1016/j.apnum.2020.03.026.

[28] B. Mercier, J. Osborn, J. Rappaz, and P.-A. Raviart, *Eigenvalue approximation by mixed and hybrid methods*, Math. Comp., 36 (1981), pp. 427–453, https://doi.org/10.2307/2007651.

[29] J. E. Osborn, *Approximation of the eigenvalues of a nonselfadjoint operator arising in the study of the stability of stationary solutions of the Navier-Stokes equations*, SIAM J. Numer. Anal., 13 (1976), pp. 185–197, https://doi.org/10.1137/0713019.

[30] P.-A. Raviart and J. M. Thomas, *A mixed finite element method for 2nd order elliptic problems*, in Mathematical aspects of finite element methods (Proc. Conf., Consiglio Naz. delle Ricerche (C.N.R.), Rome, 1975), 1977, pp. 292–315. Lecture Notes in Math., Vol. 606.

[31] J. E. Roberts and J.-M. Thomas, *Mixed and hybrid methods*, in Handbook of numerical analysis, Vol. II, Handb. Numer. Anal., II, North-Holland, Amsterdam, 1991, pp. 523–639.

[32] G. Savaré, *Regularity results for elliptic equations in Lipschitz domains*, J. Funct. Anal., 152 (1998), pp. 176–201, https://doi.org/10.1006/jfan.1997.3158.